Influence of circular RNA topology on microRNA stability

Federico Fuchs Wightman[1, 2*], Jerónimo Lukin[3*], Sebastián Giusti[3], Laureano Bragado[1, 2], Berta Pozzi[4], Paula González[5], Juan P. Fededa[5], Damián Refojo[3#] & Manuel de la Mata[2, 6#]

[1]Universidad de Buenos Aires, Facultad de Ciencias Exactas y Naturales.

[2]CONICET-Universidad de Buenos Aires, Instituto de Fisiología, Biología Molecular y Neurociencias (IFIBYNE), Buenos Aires, Argentina.

[3]Instituto de Investigación en Biomedicina de Buenos Aires (IBioBA) - CONICET - Partner Institute of the Max Planck Society, Godoy Cruz 2390, C1425FQD Buenos Aires, Argentina.

[4]Institute of Cell Biology, University of Bern, Bern, Switzerland.

[5]Instituto de Investigaciones Biotecnológicas "Dr. Rodolfo A. Ugalde", IIB-UNSAM, IIBIO-CONICET, Universidad Nacional de San Martín, Buenos Aires, Argentina.

[6]Universidad de Buenos Aires, Facultad de Ciencias Exactas y Naturales. Departamento de Fisiología, Biología Molecular y Celular.

[*]Contributed equally.

[#]Correspondence: drefojo@ibioba-mpsp-conicet.gov.ar, mmata@fbmc.fcen.uba.ar.

Abstract

Circular RNAs (circRNAs) have been proposed to “sponge” or block microRNAs, a property shared with linear RNAs. Alternatively, certain RNAs induce microRNA destruction through the process of Target RNA-Directed MicroRNA Degradation (TDMD). Whether both linear and circular transcripts are equivalent in driving TDMD is unknown. Here we show that RNA topology is critical for TDMD. Through a novel system that expresses a circRNA while reducing the co-expressed cognate linear RNA, we demonstrate that circRNAs cannot induce TDMD. Interestingly, this is attributed to the circular RNA topology and not to its sequence, which is TDMD-competent in its linear form. Similarly, based on the previous knowledge that CDR1as/ciRS-7 circular RNA protects miR-7 from Cyrano-mediated TDMD, we demonstrate that depletion of CDR1as/CirS-7 reduces mir-7 levels, while overexpression of an artificial

linear version of CDR1as/ciRS-7 drives TDMD. By analyzing RNA sequencing data of a neuron differentiation system, we suggest that circRNA-mediated microRNA stabilization is widespread. Our results support a model in which circRNAs, unlike linear mRNAs, lead to a topology-dependent TDMD evasion, aiding in the stabilization of specific microRNAs.

Keywords: circRNA/microRNA/TDMD

Introduction

Circular RNAs (circRNAs) are long known regulatory RNAs that have gained remarkable attention since the first reports that highlighted their high diversity and abundance (Memczak *et al*, 2013; Hansen *et al*, 2013; Salzman *et al*, 2013; Jeck *et al*, 2013). CircRNAs are covalently closed structures that originate from pre-mRNA backsplicing and therefore lack a poly-A tail and 5'-cap. As a result, given that these terminal modifications are the entry points for the microRNA (miRNA) effector machinery (Bartel, 2018; Jonas & Izaurralde, 2015), circRNAs seem largely immune to miRNA silencing. Furthermore, although current knowledge points towards a diversity of both nuclear and cytoplasmic functions for different individual circRNAs, several findings have suggested that some circRNAs regulate gene expression by working as miRNA "sponges" (Chen, 2020; Xiao *et al*, 2020; Hanan *et al*, 2020).

Whether circRNAs act on miRNAs by blocking them functionally, affecting their stability, or a combination of both remains to be determined. In particular, it is unclear whether circRNAs are active in driving Target Directed MicroRNA Degradation (TDMD), a mechanism that has emerged as central in affecting miRNA turnover. During TDMD, targets with extensive base-pair complementarity towards the 3' end of the miRNA –i.e. displaying no more than 3 mismatches in addition to a central bulge– lead to miRNA degradation, reversing the logic of canonical miRNA target silencing by which the target RNA is conventionally degraded (Ameres *et al*, 2010b; Cazalla *et al*, 2010a; Marcinowski *et al*, 2012; Fuchs Wightman *et al*, 2018). TDMD induces a conformational change on Argonaute (AGO) proteins that leads to their poly-ubiquitination and degradation, rendering the specifically loaded miRNAs unprotected and susceptible to degradation by general nucleases (Shi *et al*, 2020; Han *et al*, 2020). Unlike sponging, TDMD-inducing targets act catalytically even at sub-stoichiometric levels, resulting in the most selective and potent miRNA degradation mechanism described to date and which seems to explain the half-lives

58 of most naturally unstable miRNAs (de la Mata *et al*, 2015; Denzler *et al*, 2016; Kleaveland *et al*, 2018; Shi
59 *et al*, 2020). A priori, the circular topology of circRNAs should not represent an impediment to regulating
60 miRNAs through TDMD, and circRNAs' high stability could even be an advantage for this activity.
61 Nevertheless, to date no circRNA has been described to drive TDMD and the only available evidence
62 indicates that circRNAs might instead lead to miRNA stabilization (Piwecka *et al*, 2017; Chen *et al*, 2019).
63 CircRNAs are typically coexpressed with their cognate linear RNAs from the common host genes.
64 However, the circRNA over linear ratio occurs in different proportions, with a subset of circRNAs
65 reaching higher levels than their cognate linear isoforms (Chen, 2020). To reveal insights into circRNA-
66 specific functions and mechanisms, a plethora of publications have relied on circRNA overexpression
67 using various inverted repeat-containing vectors (Memczak *et al*, 2013; Zhang *et al*, 2014; Conn *et al*,
68 2015; Liang & Wilusz, 2014; Kramer *et al*, 2015; Li *et al*, 2017; Liu *et al*, 2019; Hansen *et al*, 2013; Guarnerio
69 *et al*, 2019; Litke & Jaffrey, 2019). Yet, the capability of plasmid-based methods to overexpress
70 exogenous circRNAs free from overlapping, "leaky" linear RNA expression remains questionable. Thus,
71 attributing any observed effects to the overexpressed circRNA while not rigorously controlling for the
72 potential role of the undesired coexpressed linear transcripts represents a potential pitfall (Pamudurti
73 *et al*, 2017; Kristensen *et al*, 2019; Chen, 2020; Dodbele *et al*, 2021).
74 A key general question in the field that remains largely unanswered, is whether the circular
75 nature of circRNAs is intrinsically or mechanistically linked to their molecular functions. In this study we
76 aimed to elucidate whether linear and circular target topologies function differently to affect miRNA
77 stability and function. Using a strategy that allows us to express an artificial circRNA with minimal
78 expression of the counterpart linear transcript, we showed that the circular RNA, as opposed to the
79 linear form, is unable to induce TDMD. We also examined the well described CDR1as/ciRS-7-miR-7-
80 Cyrano network of noncoding RNAs, where the lncRNA Cyrano destabilizes miR-7-5p through TDMD
81 (Kleaveland *et al*, 2018), while the circRNA CDR1as/ciRS-7 yields a protection on miR-7-5p (Piwecka *et al*,
82 2017). We show that expression of an artificially linear version of CDR1as/ciRS-7 triggers TDMD and is
83 unable to rescue the endogenous circRNA loss of function, demonstrating that the circular topology of
84 CDR1as/ciRS-7 is crucial for the evasion of TDMD. Finally, we show that interactions between circRNAs
85 and miRNAs might lead to more general phenomenon of miRNA stabilization, representing a
86 potentially widespread mechanism during neuron-like differentiation.

87

88 # Results

89 ## Artificial circRNA expression

90 In order to compare the effect of circular and linear RNAs on microRNA stability, we designed
91 constructs capable of expressing high levels of either linear transcripts or artificial circRNAs
92 encompassing segments of identical primary sequence (Figure 1A). Both the linear and circular RNAs
93 contain 4 binding sites for a candidate miRNA (miR-132) with proven TDMD-competent sequence
94 complementarity (de la Mata *et al*, 2015) (Figure S1A). To express the circRNA, we followed a strategy
95 consisting of inserting acceptor and donor splice sites flanking the segment of the transcript to be
96 circularized, plus Alu reverse complementary sequences (RCS) from the introns of a naturally
97 circularized RNA (human ZKSCAN1 exons 2 and 3 respectively), (Figure 1A) (Liang & Wilusz, 2014). In
98 order to preferentially enrich the expression of the circular over the linear variant in neurons, we
99 introduced perfectly matched sites against an endogenous neuronal miRNA (miR-124) which are lost
100 after RNA processing in the backspliced circular product but remain present in the linear RNA isoform,
101 thus rendering the linear –but not the circular– RNA form susceptible to AGO2 slicing (Figure 1A). As a
102 TDMD positive control, we expressed a linear transcript with identical sequence to the artificial circRNA
103 construct, but lacking the splice sites and the reverse complementary flanking introns that induce
104 circularization (Liang & Wilusz, 2014) (Figures 1B and S1A). The latter constructs have been proved
105 effective in triggering TDMD in primary neurons (de la Mata *et al*, 2015). All constructs were packed into
106 lentiviral vectors and used to transduce mouse primary neurons.

107 To confirm that the expressed circRNA had covalently linked ends and was therefore resistant to
108 RNA exonuclease digestion, we treated total RNA samples with RNase R. We observed that the artificial
109 circRNA was significantly less susceptible to the digestion than the linear transcript, supporting a
110 circular structure (Figure S1B). Next, to rule out artifacts that could be caused by template switching
111 during cDNA synthesis and that could serve as templates for the divergent primers -designed to amplify
112 across the artificial circRNA backspliced junction- (Figure 1A, primer pair 1), we performed the PCR from
113 cDNAs obtained with two different reverse transcriptases (MMLV-RT & Superscript II). Amplification
114 from both cDNAs produced identical PCR products with identical sequences spanning the predicted
115 backsplicing junction (Figure S1C). Because the two RT enzymes are unlikely to jump at the exact same

116 sequences during a putative template switching event, we conclude the transcripts produced from our
117 expression system are bona fide circRNAs.

118 In order to validate that our constructs expressed a single circRNA species and no concatemers
119 or other spurious by-products, we performed Northern blot analysis in RNase R treated or untreated
120 samples from HEK293T cells, a cell line where miR-124 is not expressed endogenously. We observed
121 that both artificial circRNA constructs bearing either perfect or seed-mutant sites for miR-124, rendered
122 two bands: an RNase R-resistant circRNA product and an RNase R-sensitive linear RNA form. The linear
123 RNA construct produced a single band (Figure S1D). Importantly, digital quantification of northern blot
124 bands correlated strictly with the RT-qPCR measurements using primers to amplify either the circular
125 isoform exclusively (Figure 1A, primer pair 1) or both the linear and circular isoforms combined –
126 hereafter referred to as Total Output (TO)– (Figure 1A, primer pair 2), further validating the latter method
127 for subsequent analysis (Figure S1E). Finally, to validate that our strategy was successful at expressing a
128 circRNA while selectively degrading its counterpart linear transcript by means of miR-124, a microRNA
129 specifically and highly expressed in neurons, we compared the expression products of the artificial
130 circRNA constructs bearing either perfect or seed-mutant miR-124 binding sites targeting the linear
131 isoform (Figure S1A). To that end we transduced the circRNA artificial constructs into mouse primary
132 neurons and performed RT-qPCR using both the primers described above plus additional primers to
133 amplify the linear isoform exclusively (Figure 1A, primer pair 3). Remarkably, we observed that our
134 strategy led to a potent degradation of "leak" linear RNA without affecting the circRNA levels (Figure
135 1B). Furthermore, circRNA levels produced from the circRNA-expressing construct were exceedingly
136 higher than from the construct expressing the linear RNA (TDMD positive control), while resulting in
137 equivalent total output levels (Figure 1C). Altogether, these results confirm that our system is effective
138 in expressing circRNAs while reducing the levels of their cognate linear RNAs, making it a generally
139 useful tool in experiments aimed at dissecting circRNA function.

140

141 **Artificial circRNAs are incapable of triggering TDMD**

142 In order to explore whether linear and circular target topologies function differently to affect
143 miRNA stability through TDMD, we determined the extent to which a circular RNA topology can impact
144 miRNA stability via TDMD in neurons, a cell type known to display a potent TDMD effect (de la Mata *et*

145 *al*, 2015). To this end we transduced primary neurons with either linear or circRNA expression constructs
146 bearing TDMD-competent (bulged) or seed-mutant binding sites for miR-132, and measured miR-132
147 levels by an RT-qPCR Taqman assay. Whereas the linear TDMD inducer was capable of effectively
148 destabilizing miR-132, its circularized version showed no effect on miRNA stability even when both
149 constructs reached similar total RNA levels (Figures 1C and 2A).
150 In order to determine whether the observed differential effect could be attributed to the inability of the
151 circular RNA to bind to the RISC complex, we set out an RNA immunoprecipitation experiment (RIP) by
152 specifically pulling-down AGO2 and isolating all copurifying RNA species. To this end, we coexpressed
153 FLAG/HA-AGO2 in HEK293T cells together with the different circular RNA constructs followed by
154 immunoprecipitation and RT-qPCR analysis. We observed that the artificial circRNA was effectively
155 pulled down together with AGO2 only when carrying bulged sites for miR-132 but not if the sites were
156 mutated at the miRNA seed-binding region (Figures 2B and S2A-B). These results demonstrate that the
157 circular RNA is indeed able to specifically bind to the RISC complex, ruling out that defects in circRNA-
158 AGO2 binding could account the observed lack of TDMD activity.
159 In order to exclude the possibility that the observed differences were a trivial consequence of an
160 aberrant localization of the circRNA relative to the linear isoform (Chen, 2020), we performed a
161 purification of nuclear and cytoplasmic subcellular fractions. Our results showed that the artificial
162 circRNA accumulates in the cytoplasm at similar proportions relative to the linear control and is only
163 slightly lower in the nuclear compartment (Figures 2C and S2C-D), suggesting that the inability of the
164 circRNA to trigger TDMD is not related to it being retained in the nucleus.
165

166 **Circular topology of CDR1as/ciRS-7 is necessary to protect miR-7 from TDMD**

167 To answer whether the inability to trigger TDMD was restricted to our circRNA expression system
168 or if it may actually be observed for other known endogenous circRNAs as well, we studied the case of
169 the CDR1as/ciRS-7-miR-7 interaction (Hansen *et al*, 2011, 2013; Memczak *et al*, 2013). To determine
170 whether the circular topology of CDR1as/ciRS-7 has a role in modulating miR-7 levels, we designed tools
171 to manipulate endogenous CDR1as/ciRS-7 levels in rodent primary neurons (Fellmann *et al*, 2013). In
172 order to knock down CDR1as/ciRS-7 we engineered a lentiviral vector to express a specific shRNAmiR
173 (shCDR1as) and transduced it in primary neurons at high efficiency. Interestingly, the effective

174 CDR1as/ciRS-7 knockdown achieved did not increase miR-7 levels as expected had CDR1as/ciRS-7 been
175 an active inducer of TDMD on this miRNA. On the contrary, and in line with previous evidence (Piwecka
176 *et al*, 2017), CDR1as/ciRS-7 knockdown reduced miR-7 levels, consistent with a stabilization role of the
177 circRNA on this miRNA (Figure 3A).

178 To determine whether the observed effect was dependent on CDR1as/ciRS-7's circular topology,
179 we attempted to rescue the CDR1as/ciRS-7 knockdown with the expression of an artificial linear version
180 of CDR1as/ciRS-7 –linCDR1as– lacking the shCDR1as target site. Interestingly, the drop of miR-7 levels
181 caused by the knockdown of the endogenous CDR1as/ciRS-7, could be neither rescued nor enhanced
182 by co-expressing the linear CDR1as/ciRS-7, even though the artificial linCDR1as reached expressions
183 levels similar to those of endogenous CDR1as/ciRS-7 in control cells (Figure 3A). Remarkably, expressing
184 linCDR1as alone –without knocking down endogenous CDR1as/ciRS-7 caused a significant
185 destabilization of miR-7 (Figure 3B), consistent with TDMD being driven by the RNA expressed under an
186 artificial linear RNA topology. Careful inspection of the miR-7 sites present in CDR1as/ciRS-7 showed
187 that no less than 5 of them indeed exhibit a base pairing complementarity compatible with a TDMD-
188 competent architecture (Figure S3A). Importantly, the observed effect on miR-7 caused by
189 overexpression of linear linCDR1as did not correlate with any variation of the endogenous levels of
190 (circular) CDR1as/ciRS-7, arguing against potential indirect effects due to overexpression of the
191 transgene (Figure S3B).

192 As an orthogonal strategy to reduce CDR1as/ciRS-7 levels and rule out potential off target or
193 indirect effects caused by the shCDR1as, we used CRISPR/Cas9 genome editing to mutate the splicing
194 sites of the endogenous CDR1as/ciRS-7 gene. To that end we expressed two sgRNAs against both donor
195 and acceptor splice sites of CDR1as/ciRS-7 respectively (Figure S3C). Despite an overall lower efficacy in
196 CDR1as/ciRS-7 knockdown reached through CRISPR/Cas9 editing compared to the shCDR1as, we
197 observed a similar effect consistent with CDR1as/ciRS-7 being unable to induce TDMD on miR-7 but
198 rather leading to its stabilization (Figure S3D-E).

199 To test whether miR-7 destabilization produced by CDR1as/ciRS-7 knockdown also resulted in
200 the expected upregulation of previously described mRNA targets, we measured the levels of four
201 validated miR-7 targets via RT-qPCR. We observed that all four of them were slightly upregulated upon
202 CDR1as/ciRS-7 knockdown relative to control (Figure 3C). Along the same line, reanalysis of RNA

203 sequencing data from published data further confirmed that miR-7 predicted targets (retrieved from
204 TargetScanMouse v7.1) were significantly upregulated in mouse cortex upon CDR1as/ciRS-7 knockout
205 (Figure 3D-F) (Piwecka *et al*, 2017).

206 Overall, our results show that endogenous CDR1as/ciRS-7 is unable to trigger TDMD on miR-7
207 but rather stabilizes this miRNA. Accordingly, only if expressed as an artificially linear RNA can it engage
208 in miR-7 degradation through TDMD, further supporting the notion that the natural circular/linear
209 topology, and not just the linear sequence of a RNA target, is a crucial determinant for engaging in such
210 type of regulation.

211

212 CircRNAs potentially stabilize dozens of microRNAs across neuron-like 213 differentiation

214 Based on our results, we hypothesized that circRNAs might possess the ability to influence
215 miRNA stability through evading TDMD and eventually protecting miRNAs from degradation. Yet,
216 whether this type of regulation could be a widespread phenomenon is unclear. To explore this
217 possibility, we analysed available sequencing data of miRNA, circRNA and mRNA expression from hESC
218 H9 cells both undifferentiated and differentiated into forebrain (FB) neuron progenitor cells (Chen *et al*,
219 2015; Zhang *et al*, 2016). We reasoned that this model would be appropriate to test our hypothesis from
220 the viewpoint that a significant proportion of circRNAs are regulated along neuron differentiation -with
221 upregulation being more frequent than downregulation (You *et al*, 2015; Rybak-Wolf *et al*, 2015).
222 Concomitantly, neuron-specific miRNAs are known to become more susceptible to degradation in more
223 mature neurons (Krol *et al*, 2010), a scenario where circRNAs could act by selectively regulating miRNA
224 stability. In order to consider only the biochemically supported circRNA-miRNA pairs, we used the CLIP-
225 Seq experimentally supported mRNA-miRNA, lncRNA-miRNA and circRNA-miRNA interaction networks
226 catalogued in the STARBASE v3/ENCORI database (Yang *et al*, 2011; Li *et al*, 2014) as a proxy for bona
227 fide interactions.

228 We addressed the analysis following two different but complementary approaches. The first one
229 aimed at studying the expression of the most highly "sponged" miRNAs, namely those interacting with
230 multiple and/or highly expressed circRNAs, across differentiation of hESC H9 cells into forebrain neuron
231 progenitor cells. To that end, for every expressed individual miRNA we calculated a "sponging

232 coefficient". The score was computed by multiplying the number of specific miRNA sites present on
233 each circRNA by the number of backspliced junction reads of each circRNA before differentiation,
234 resulting in the "effective" number of specific miRNA sites contributed by each circRNA. The sum of all
235 effective number of sites contributed by all circRNAs provided a measure of the total effective number
236 of sites for each individual miRNA (Figure 4A, ranked in Supplementary Data 1). The "sponging
237 coefficient" was finally obtained by normalizing this number to each miRNA's expression level before
238 differentiation (Figure 4B, ranked in Supplementary Data 1). According to this analysis, the most highly
239 "sponged" miRNAs, as defined by those with the highest "sponging coefficients", were significantly
240 upregulated across differentiation (Figure 4C). We next sought to determine whether the observed
241 correlation was a consequence of post-transcriptional stabilization of mature miRNAs and not the trivial
242 effect of changes in miRNA gene transcription rates. To that end we estimated the change in pri-miRNA
243 expression levels as a proxy for change in transcription levels of the respective miRNA genes across
244 differentiation. Interestingly, we found that the correlation between fold changes of mature miRNA and
245 pri-miRNA levels was weaker for the most highly "sponged" miRNAs than for the more poorly "sponged"
246 miRNAs, arguing for a stabilization and not a transcriptional effect (Figure 4D). In sum, this analysis is
247 consistent with a miRNA stabilization through the concerted interaction of individual miRNAs with
248 multiple and/or highly expressed circRNAs across differentiation.

249 As a complementary approach, we aimed at analysing the expression of the potentially most
250 highly "sponging" circRNAs, namely those potentially interacting with multiple miRNAs across
251 differentiation into forebrain neuron progenitor cells. To that end we calculated the total number of
252 sites (for all miRNAs) present on each circRNA, which resulted in the total number of predicted
253 "effective" sites (Figure 4E and Supplementary Data 1). Interestingly, we observed that an increasing
254 number of effective sites present on circRNAs does not correlate with an obvious decrease in circRNA
255 fold change expression across differentiation, which is consistent with the notion that circRNAs are
256 immune to miRNA regulation (Figure 4F). The collection of miRNAs and circRNAs interacting across this
257 neuron-like differentiation might include more than a hundred miRNAs and dozens of circRNAs. In fact,
258 by focusing on the predicted most highly sponging circRNAs, this analysis further illustrates that
259 circRNAs with the highest "sponging" capacity for miRNAs lie at highly connected nodes within a

260 complex regulation network, further supporting the view that individual circRNAs might act as potential
261 scaffolds for multiple miRNAs (Figure S4A).
262

263 ## Discussion

264 A long-lasting and largely unresolved question in the field is whether circRNAs' topology, i.e.
265 their circular nature, is intrinsically relevant for them to exert their molecular actions. Alternatively, the
266 circular form of some circRNAs might have been evolutionarily selected merely based on their
267 resistance to endonucleases that confer them special stability properties. Due to different technical
268 reasons, many of which are related to the expression systems employed, these key questions have not
269 been fully addressed so far.

270 While most experimental approaches have largely relied on knocking down or overexpressing
271 circRNAs in different organisms or cultured cells, undesirable artifacts can very commonly act as
272 confounding factors in the interpretation of the results. In particular, overexpression of circRNAs suffers
273 from a major caveat related to the unwanted linear RNA species that are inevitably co-expressed from
274 the commonly used expression vectors. This type of problem can easily lead to conclusions where
275 functions are wrongly assigned to circRNAs under circumstances where the associated linear transcripts
276 are the true functional molecules but are ignored in the experiments (Dodbele *et al*, 2021). We have
277 addressed this issue by designing a strategy that allows us to express circRNAs while keeping expression
278 of the counterpart linear product to a minimum. A similar strategy was previously reported in a different
279 context with the goal of restricting expression of transgenes to specific tissues (Brown *et al*, 2007). In
280 our hands the approach proved to work as an efficient tool to deliver high levels of circRNAs while
281 limiting the expression of the linear RNA derived from the circRNA construct (Figure 1).

282 We have exploited this tool to gain insight into the mechanism of the well-known role of
283 circRNAs in blocking miRNAs. Despite being neither prevalent nor unique to circRNAs as a class, the
284 capacity to inhibit or "sponge" miRNA silencing activity has been the most extensively documented
285 function of circRNAs (Chen, 2020; Dodbele *et al*, 2021). This abundance of papers likely obeys to
286 historical reasons, namely the fact that this was the first function to be reported for circRNAs since their
287 rediscovery during the last decade (Memczak *et al*, 2013; Hansen *et al*, 2013). In spite of this, a clear
288 picture of the mechanism by which some circRNAs act on miRNAs is still missing. For instance, it remains

289 unclear whether circRNAs act on microRNAs simply by blocking their function and/or by affecting their
290 stability. In this sense, although it has been speculated that circRNAs might trigger TDMD like linear
291 RNAs, this premise was never formally and experimentally tested so far (Gasparini *et al*, 2020). Our data
292 suggest the opposite: even when expressed at comparable levels, artificial circular RNAs of identical
293 sequence to those of TDMD-inducing linear RNAs, prove incapable of inducing TDMD (Figure 2). This is
294 largely recapitulated by the endogenous circRNA CDR1as/ciRS-7 which cannot trigger TDMD on miR-7
295 –in fact it leads to its stabilization as discussed below– unless artificially expressed as a linear RNA.

296 The fact that the protection of miR-7 exerted by CDR1as/ciRS-7 was not recapitulated by our
297 artificial circRNA on miR-132, might be explained by the emergent properties of the CDR1as/ciRS-7-miR-
298 7-Cyrano network. Based on this idea, the stabilization of miR-7 might emerge from the inability of
299 CDR1as/ciRS-7 to drive TDMD in combination with its preserved ability to bind and compete for miR-7,
300 ultimately shielding the exceptionally potent TDMD activity driven by Cyrano on miR-7 (Kleaveland *et*
301 *al*, 2018). A similar reasoning might apply to the fact that the artificial (linear) linCDR1as, when expressed
302 in combination with the knockdown of endogenous (circular) CDR1as/ciRS-7, does not produce any
303 additional reduction of miR-7 levels: under these conditions, an unleashed Cyrano-driven TDMD activity
304 acting on miR-7 might reach a limit in miR-7 degradation rate which cannot be further enhanced by an
305 additional TDMD-competent target such as linCDR1as. In the presence of CDR1as/ciRS-7, the system
306 would be set to intermediate miR-7 degradation rates which could be further enhanced by other TDMD-
307 competent RNAs such as linCDR1as (see model in Figure S4B). Notably, a similar protection
308 phenomenon has been observed in a prostate cancer cell line, where knockdown of circCSNK1G3
309 bearing binding sites for miR-181b/d decreased their abundance, while circCSNK1G3 overexpression
310 increased it (Chen *et al*, 2019).

311 The molecular basis explaining the functional differences between circRNAs and their cognate
312 linear transcripts in triggering TDMD, might obey to the structural properties affected by the circular-
313 linear topology. Based on a previous report, whereas circRNAs inhibit PKR-mediated innate immune
314 responses, their cognate linear counterpart transcripts cannot. The explanation behind this
315 phenomenon seems to be the inherent ability of circRNAs to fold into more stable short local secondary
316 structures compared to their linear counterpart transcripts. This in turn seems to lead to a more stable
317 interaction between circRNAs and PKR (Liu *et al*, 2019). Based on similar principles –but with an opposite

318 outcome– the greater tendency of circRNAs to form secondary structures could confer them an extra
319 rigidity that could ultimately limit their capacity to drive TDMD. This seems in agreement with previous
320 reports showing that an extended miRNA:target basepairing *per se* is not enough to trigger TDMD:
321 miRNA binding must also occur within a conformationally flexible region of the target for TDMD to be
322 active (Pawlica *et al*, 2016; Fuchs Wightman *et al*, 2018; Li *et al*, 2021). In line with this idea, two in-depth
323 studies have contributed to our understanding of TDMD by pinpointing the ubiquitin ligase ZSWIM8 as
324 a mediator of the mechanism (Shi *et al*, 2020; Han *et al*, 2020). These findings showed that the binding
325 of TDMD-competent target RNAs drives a conformation change on AGO proteins (loaded with specific
326 miRNAs) that leads to their poly-ubiquitination and degradation, leaving the specific miRNAs
327 unprotected and susceptible to degradation by general nucleases. The extra rigidity of circRNAs could
328 preclude the conformational change of AGO, thus bypassing TDMD while remaining bound to the RISC
329 complex. A recent report might be consistent with this view by showing differences between the
330 thermodynamic properties of linear and circular RNA in binding to complementary short RNAs,
331 favouring a model where circRNAs might bind to miRNAs more efficiently than their cognate linear
332 RNAs (Petkovic *et al*, 2021).

333 An alternative explanation could relate to the differential ability of distinct RNA species in
334 recruiting TDMD machinery factors such as ZSWIM8. In that sense, several characteristics of circRNAs
335 could be critical such as their lack of capping and poly-A tails, although the latter seems dispensable for
336 TDMD based on the fact that HSUR-1, which lacks a poly-A tail, effectively drives TDMD on miR-27
337 (Cazalla *et al*, 2010b; Pawlica *et al*, 2016). Additionally, specific sequence elements within linear
338 transcripts are required for TDMD. For instance, both the miR-7 and miR-17 binding sites that exist
339 within known TDMD-inducing targets (Cyrano and HCMV's UL144-145 respectively), depend on
340 sequences that are located outside of the miRNA site *per se* for efficiently triggering of TDMD (Lee *et al*,
341 2013; Han *et al*, 2020; Kleaveland *et al*, 2018). Such sequences might be absent or simply occluded
342 within the more highly structured circRNAs, possibly explaining their observed inability to drive TDMD.

343 An increasing number of TDMD natural examples have arisen in the past few years, including
344 both endogenous targets capable of destabilizing specific miRNAs and viral transcripts which in doing
345 so facilitate infection (Ameres *et al*, 2010a; Cazalla *et al*, 2010b; Li *et al*, 2017; Bitetti *et al*, 2018; Ghini *et*
346 *al*, 2018; Li *et al*, 2021; Simeone *et al*, 2022). Furthermore, the discovery that TDMD is more widespread

347 than initially thought suggests that many more instances of endogenous TDMD will be discovered (Shi
348 *et al*, 2020; Han *et al*, 2020). In this scenario, circRNAs' capacity to evade such regulation could confer
349 them an advantage in regulating miRNA stability even when involving highly complementary pairing
350 architectures that would otherwise drive TDMD in the context of linear RNAs. As a result, circRNAs may
351 achieve an indirect stabilization of miRNAs by specifically sequestering and rendering them unavailable
352 for TDMD. This type of regulation would in turn be compatible with a potential reversibility of circRNA's
353 inhibitory function on miRNAs.

354 Interactions between miRNAs and competing-endogenous RNAs (ceRNAs) have received a
355 broad attention in the recent years as they might represent a mechanism of miRNA inhibition (Tay *et al*,
356 2014). However, due to stoichiometry considerations, the likelihood that individual ceRNAs titrate the
357 total amount of miRNA available for target repression seems limited (Denzler *et al*, 2014, 2016; Jens &
358 Rajewsky, 2015; Bosson *et al*, 2014; Pinzon *et al*, 2017). Instead, models where multiple ceRNAs regulate
359 single miRNAs have been favoured (Ameres & Zamore, 2013; Dodbele *et al*, 2021). The case of
360 CDR1as/ciRS-7-miR-7 pair might represent an outstanding example functioning in an analogous way:
361 CDR1as/ciRS-7 is a highly expressed circRNA with > 60 evolutionarily conserved miR-7 binding sites
362 based on previous reports (Memczak *et al*, 2013; Hansen *et al*, 2013) (67 predicted sites for miR-7 in
363 humans based on the STARBASE/ENCORI database), significantly exceeding the average number of
364 sites annotated for circRNAs (based on Starbase/ENCORI database, see Supplementary Data 2). On the
365 other hand, while CDR1as/ciRS-7 is highly expressed in human, rat and mouse brain, miR-7 tends to
366 display medium to low expression. Our results favour a model where the concerted interaction of
367 multiple circRNAs with individual miRNAs seems the most likely and relevant scenario in regulating
368 miRNA stability. Interestingly, among the miRNAs that are upregulated upon ZSWIM8 knockdown in
369 mouse induced neurons (Shi *et al*, 2020), two belong to the most "sponged" miRNAs according to our
370 analysis (miR-7 and also miR-409-3p), suggesting that such type of regulation might be acting in neuron
371 differentiation and possibly in pathophysiological conditions.

372 A complex and yet unresolved aspect of the role of circRNAs in regulating miRNAs relates to our
373 inability to predict their outcome on canonical miRNA silencing activity. In this sense, depending on the
374 relative binding site architectures and the relative stoichiometries of the molecules involved, different
375 outcomes may be expected. For instance, miRNA stabilization could lead to greater average target

376 repression due to an increased abundance of the miRNA. This is indeed observed for miR-7 targets in
377 primary neurons upon CDR1as/ciRS-7 KD (Figures 3F-H) (Piwecka *et al*, 2017). However, miRNA
378 stabilization may also be accompanied by an overall tight blockade of miRNA silencing activity, leading
379 to opposite outcomes in different contexts. Such could be the case of miR-181b/d in a prostate cancer
380 model, where its decreased abundance upon circCSNK1G3 knockdown (resembling the case of miR-7
381 and CDR1as/ciRS-7), leads to downregulation of miR-181b/d predicted targets (Chen *et al*, 2019)
382 (Figures S3G and H). Eventually, more in-depth knowledge of the players involved, their dynamics and
383 relative stoichiometries will help us understand the emergent properties arising from different systems
384 and the full potential and adaptive value of circRNAs in miRNA regulation.
385

386 # Materials and methods

387 ## Plasmid construction

388 Unless otherwise specified, the lentiviral vectors are based on pRRLSIN.cPPT.SYN.WPRE (de la Mata *et al*,
389 2015).
390 Linear CDR1as/ciRS-7 was amplified by PCR from rat genomic DNA (see primers at Supplementary Table
391 1). Following gel purification (QIAquick Gel Extraction Kit), and cloning into pCR II-Blunt-TOPO
392 (ThermoFisher) it was then subcloned into pRRLSIN.cPPT.SYN.WPRE. The linear CDR1as/ciRS-7 version
393 lacking the shCDR1as target site -linCDR1as^{671}- was done by PCR amplification and re-cloning in the
394 original backbone (Supplementary Table 1), eliminating the BamHI-SalI segment containing the full
395 linCDR1as. The linear transcript used as a negative control consists of mCherry carrying four mutated
396 sites for miR-7, obtained by eliminating the miR-132 sites (NheI-SalI) from an already published linear
397 TDMD inducer (de la Mata *et al*, 2015) and adding miR-7 sites by Gibson Assembly (Gibson *et al*, 2009)
398 and a gBlock (Integrated DNA Technologies, see sequence at Supplementary Table 1).
399 The pri-miR-132 and pri-miR-124 expressing constructs were made by eliminating the BamHI-BsrGI
400 portion of pRRLSIN.cPPT.SYN.WPRE and amplifying the pri-miRs (Supplementary Table 1) from
401 miRNASelectTM pEGP-mmu-mirna expression vectors (Cell Biolabs).
402 The shRNAmiR (shCDR1as) is an engineered version miR-671 -previously described as a natural
403 CDR1as/ciRS-7 regulator (Piwecka *et al*, 2017; Kleaveland *et al*, 2018)- designed to be fully
404 complementary to the circRNA and maximizing its slicing (Figure 3A). The shCDR1as lentiviral vector

405 was constructed by removing the pri-miR from one of the previously made vectors using BamHI-NheI
406 (Supplementary Table 1), and inserting a synthetic DNA (gBlock gene fragment, IDT) by Gibson
407 Assembly (Gibson *et al*, 2009).
408 Plasmid for artificial circRNA expression was constructed using the same procedure, using gBlocks
409 (Integrated DNA Technologies) with the ZKSCAN1 upstream and downstream introns (Liang & Wilusz,
410 2014) flanking mCherry and miR-132 sites (de la Mata *et al*, 2015). We later added the sites for miR-124
411 by exchanging mCherry from a linear TDMD inducer, XhoI, for the circularizing portion XhoI-SalI. Finally,
412 we swapped the SYN promoter, XbaI-BamHI, for TREp (see Figure 1A and Supplementary Table 1). As a
413 positive control for degrading miR-132, we used a previously described linear TDMD inducer consisting
414 of mCherry with miR-132 sites (de la Mata *et al*, 2015). The tetracycline-inducible promoter (TREp) was
415 amplified from the plasmid SYN-Tetoff-GFP (Gascón *et al*, 2008). Three different variants of the artificial
416 circRNA were made: one with 4x TDMD-inducing (bulged) miR-132 sites in the circularizing segment
417 and 4x perfectly matched sites for miR-124 only present in the linear isoform; the other two variants
418 have either miR-132 or miR-124 mutated sites.
419 The lentiviral vector driving expression of FLAG/HA-AGO2 (human) from the Syn promoter (pLV-FLAG-
420 HA_AGO2) was generated by amplifying FLAG/HA-AGO2 from pIRESneo-FLAG/HA AGO2 (Addgene
421 plasmid 10822).
422 The construct for CRISPR/Cas9 genome editing of CDR1as/ciRS-7 splicing sites is based on lentiCRISPR
423 v2 (Addgene plasmid 52961), following the Zhang Lab protocol (Sanjana *et al*, 2014; Shalem *et al*, 2014).
424 See primers at Supplementary Table 1.
425

426 HEK293T culture and transient transfection

427 HEK293T cells were available in our institute. Cells were tested for mycoplasma contamination and only
428 clean stocks were further used for our experiments. Cells were grown in DMEM-F12 (Gibco)
429 supplemented with 10% (v/v) FCS and 25 U/mL Penicillin-Streptomycin (Gibco) and were plated for
430 transfection at 100,000 cells/well on 24-well plates. One day after plating, cells were transfected using
431 the PEI method with the following plasmids: the artificial circRNA expressing construct, the linear TDMD
432 inducers and/or the FLAG/HA-AGO2 plasmid. Co-transfected were the pri-miR-132, pri-miR-124 and/or

433 tTA expressing vectors when appropriate. The optimal amount of pri-miR-132 transfected had been
434 previously described (de la Mata *et al*, 2015).
435

436 **Lentivirus production and transduction**

437 Recombinant lentiviral particles were produced in HEK293T cell line. Cells were co-transfected using the
438 PEI method with the lentiviral expression vector and two packaging vectors: pMD2.G (Addgene plasmid
439 12259), a plasmid expressing the VSV-G envelope gene, and pCMVR8.74 (Addgene plasmid 22036), a
440 plasmid expressing the gag/pol genes (2nd generation lentiviral packaging plasmid). The supernatants
441 containing the viral particles were collected 48–72 h after transfection and concentrated using
442 centrifugal filter units (Amicon Ultra-15, molecular weight cutoff 100 kDa, Millipore Cat. # UFC910024).
443 Viral titers were determined semi-quantitatively by serial dilution on primary hippocampal neurons and
444 observation of GFP/mCherry infected cells. In turn, MOIs correlated well with the measured GFP mRNAs,
445 allowing us to achieve similar expression levels across several experiments by infecting at similar MOIs.
446

447 **Animals used in this study**

448 All animal tissues used in this study were obtained under experiment protocol no. No.2020-04-DR with
449 the approval from the Comisión Institucional para el Cuidado y Uso de los Animales de Laboratorio
450 (CICUAL) at the Instituto de Investigación en Biomedicina de Buenos Aires (IBioBA) – CONICET – Partner
451 Institute of the Max Planck Society.
452

453 **Neuronal cultures and lentiviral transduction**

454 Cortical and hippocampal neurons were dissected from embryonic day 16.5 and 18.5 (E16.5 and
455 E18.5) respectively CD1 embryos of mixed sex. Culture preparation was performed as previously
456 described (Giusti *et al*, 2014; Vogl *et al*, 2015). Briefly, cortex from CD1 mouse embryos were dissected
457 and a neuronal suspension was prepared through Trypsin digestion and mechanical disruption of the
458 tissue. Neurons were plated in 24 multi-well plates at a density of 80cells/mm2 (150.000 cells per well)
459 and maintained in Neurobasal-A media (ThermoFisher) with 2% B27 and 0.5 mMGlutaMAX-I
460 (ThermoFisher) at 37 °C and 5% CO2. CD1 mice for neuronal cultures were provided by our Specific
461 Pathogen Free Animal Facility.

462 The euthanasia of the animals to generate primary neuronal cultures was performed under
463 experiment protocol no. 2020-04-DR which was evaluated by the Institutional Animal Care and Use
464 Committee of the IBioBA-CONICET according to the Principles for Biomedical Research involving
465 animals of the Council for International Organizations for Medical Sciences and provisions stated in the
466 Guide for the Care and Use of Laboratory Animals.

467 Neurons were transduced 4-7 days after plating (DIV4-7) with either of the following lentiviral
468 constructs: linCDR1as, linCDR1as^{671-}, shCDR1as, the linear control or a combination of these,
469 appropriately described in Results and Figures. The vectors driving each of the artificial circRNAs
470 expressions were transduced in combination with a lentiviral construct expressing the tetracycline-
471 controlled transactivator protein (LV-Syn-tTA). RNA was extracted at DIV11 as indicated below.

472

473 **FLAG/HA-AGO2 transfection and immunoprecipitation (AGO2 RIP)**

474 The FLAG/HA-AGO2 expressing plasmid was transfected into HEK293T cells as described above.
475 Immunoprecipitation of FLAG/HA-AGO2 was performed with Anti-FLAG M2 Magnetic Beads (Sigma.
476 Cat # M8823). Beads were washed twice with TBS buffer (50 mM Tris HCl, 150 mM NaCl, pH 7.4). For each
477 immunoprecipitation (IP), one 6-cm plate with 50% confluency was used. Cells were washed once with
478 cold PBS and lyzed in 500 µl of lysis buffer [50 mM Tris–HCl pH 7.5, 150mM NaCl, 1% (v/v) TRITON X-100,
479 1 mM EDTA, containing protease inhibitors (cOmplete, EDTA-free Protease Inhibitor Cocktail, Roche)
480 and RNase inhibitor (Invitrogen)]. The lysates were incubated 30 minutes on ice, cleared by
481 centrifugation at 16,000 g for 10 minutes at 4 degrees and mixed with the washed beads. After 2 hours
482 of rotation at 4 degrees, the beads were washed three times with TBS buffer. As a control for the IPs,
483 non-transfected HEK293T cells were used. FLAG/HA-AGO2 expression and immunoprecipitation
484 efficiency were determined by Western blot using anti-HA antibody (clone 3F10, Roche). Monoclonal
485 antibody against Actin was purchased from Chemicon (MAB1501). Antibodies against α-Tubulin and
486 Histone-3 were purchased from Santa Cruz Biotechnology. RNA was extracted by adding Trizol reagent
487 (Invitrogen) directly on the beads.

488

489 **Subcellular fractionation**

490 Briefly, the artificial circRNA expressing construct and the linear control were transfected into HEK293T
491 cells as described above, in 6-well plates at 50% confluency. After 48 hours, cells were harvested using
492 500 μl of PBS, transferred to a microcentrifuge tube and centrifuged at 500 g for 5 minutes. The
493 supernatant was discarded, and the pellet resuspended in 350 μl of PBS plus 0.1% NP-40 (IGEPAL). 150
494 μl were separated and called TOTAL fraction. The remaining volume was centrifuged for 10 seconds at
495 10,000 rpm. 150 μl of the supernatant were separated and called CYTOPLASM fraction. The pellet was
496 resuspended in 150 μl of PBS plus 0.1% NP-40 (IGEPAL) and centrifuged again at 10,000 rpm. The
497 supernatant was discarded, and the pellet resuspended in 150 μl of PBS plus 0.1% NP-40 (IGEPAL). This
498 was called the NUCLEAR fraction.
499 Out of the 150 μl of each fraction, 75 μl were used for Western Blotting and 75 μl for RNA extraction
500 followed by reverse transcription and quantitative polymerase chain reaction (RT-qPCR).
501

502 **RNA extraction**

503 Total RNA extractions were made using Trizol reagent (Invitrogen) following the manufacturer's
504 instructions.
505

506 **RT-qPCR quantification**

507 MiRNA and U6 levels were determined by using Taqman® microRNA Assays (Applied Biosystems)
508 following the manufacturer's instructions. MicroRNA levels were normalized to U6 RNA levels. Standard
509 curves for the analyzed miRNAs and U6 RNA were performed with serial dilutions of selected cDNAs,
510 allowing calculation of relative levels. For quantification of target mRNAs, the different isoforms of the
511 artificial circRNA constructs and CDR1as/ciRS-7, total RNA was treated with RNase-free DNase I (DNA-
512 freeTM Kit, Ambion) and reverse transcribed using random hexamers and SuperScriptTM II Reverse
513 Transcriptase (Invitrogen), following the manufacturer's instructions. Target mRNA, the different
514 isoforms of the artificial circRNA constructs levels and CDR1as/ciRS-7 were determined by SYBR green
515 qPCR using a custom-made qPCR mix (Supplementary Table 2) and specific primers (detailed at
516 Supplementary Table 3). Alternatively, INBIO highway qPCR SYBR green mix was used (Ref M130).
517 Standard curves for the analyzed amplicons were done with serial dilutions of selected cDNAs, allowing
518 calculation of relative levels.

519

520 ## Northern blot analysis

521 Northern blot analysis was performed according to standard procedures (Roditi *et al*, 1987). A total
522 amount of 10 μg of RNA was loaded in each lane. The radioactively labelled probe, corresponding to
523 the mCherry CDS fragment, was prepared using the Megaprime DNA labelling kit (Amersham
524 Biosciences) according to manufacturer's instructions. The 18S RNA from the agarose gel run was used
525 as loading control. Blots were hybridized at 65° and washed in 0.2× SSC/0.1% SDS. The blots were
526 exposed to Phosphorimager screens and scanned with Typhoon FLA 7000 (GE Healthcare Life Sciences).
527 The relative intensities of the bands were measured by densitometry using ImageJ.

528

529 ## Western blot analysis

530 Protein samples were separated on 12% SDS-polyacrylamide gels and transferred to PVDF membranes.
531 Membranes were incubated with primary antibodies: anti-HA 3F10 (Rat, 1:2500), anti-Tubulin
532 (polyclonal rabbit anti βtubulin H-235 from Santa Cruz Biotechnology, 1:2500) and Histone-3
533 (polyclonal rabbit anti H3 H-0164 from Merk, 1:2500). After washing, membranes were incubated with
534 IRDye® 800CW (LI- COR Biosciences) secondary antibodies. Bound antibody was detected an Odyssey
535 imaging system (LI-COR Biosciences).

536

537 ## Statistical analysis

538 All key experiments of this study were repeated at least three times, producing biological sample sizes
539 (n) ≥3. R programming language was used to process information, visualize and design graphs, and
540 perform statistical tests. Data was normalized and scaled across experiments using Unit Length
541 Normalization. Briefly: transform x to x' by dividing each value of the feature vector by the Euclidean
542 length of the vector. Bar, line, scatter and boxplots were designed using the ggplot2 (Wickham, 2016)
543 and ggpubr packages. Statistical tests were done using base R, ggsignif
544 (https://www.rdocumentation.org/packages/ggsignif/versions/0.6.1) and/or ggpubr
545 (https://rpkgs.datanovia.com/ggpubr/index.html). For those experiments where two conditions were
546 compared, we performed one-sided t-tests, and for those with three conditions, two-sided t-tests (ns: p
547 > 0.05, *: p <= 0.05, **: p <= 0.01, ***: p <= 0.001, ****: p <= 0.0001). When comparing several miR-7

548 targets across conditions, we did a two-way ANOVA followed by Tukey multiple comparisons, showing
549 the adjusted p-values. Error bars represent the standard deviation of the mean (SEM).
550

551 **Bioinformatic analysis of circRNA-miRNA interactions**

552 Two publicly available datasets produced by the Chen Lab were combined to generate a
553 comprehensive analysis taking into account miRNA, circRNA and mRNA expression during
554 differentiation of H9 (hESC) cells to H9 forebrain neurons. From GEO Accession GSE73325 (Zhang *et al*,
555 2016) we obtained data for circRNA and mRNA expression. From GEO Accessions GSE56152 and
556 GSE63709 (Chen *et al*, 2015) we obtained data for microRNA expression. Noteworthy, although the
557 same procedure for differentiation was followed (Zhang *et al*, 2016; Chen *et al*, 2015), sequencing was
558 done on different days (D26 and D35, respectively). We realize this is suboptimal, nevertheless we
559 decided to proceed with the analysis since its goal was limited to the finding of potential candidates
560 that might be suffering from a similar type of regulation as CDR1as/ciRS-7-miR-7.
561 Data of the interaction between circRNAs and miRNAs was retrieved from Starbase/ENCORI v3 database
562 (http://starbase.sysu.edu.cn; (Yang *et al*, 2011; Li *et al*, 2014)). This particular source was selected
563 because it combines site prediction by several programs with experimental validation (e.g., by CLIP).
564 The main parameters chosen for downloading through their API were: assembly = hg19, geneType=
565 circRNA & miRNA, clipExpNum=1, program= all, programNum= 2, target= all and cellType= all.
566 A condensed spreadsheet summarizing all the previously mentioned data can be found at
567 Supplementary Data 3.
568 The analysis was done in R, briefly:

569 - The expression tables were loaded and merged using the Tidyverse package (Wickham *et al*,
570 2019), while the circRNA-miRNA interactions table was joined using the Fuzzyjoin package
571 (https://CRAN.R-project.org/package=fuzzyjoin) to consider genomic locations of both the
572 circRNAs and the miRNA sites.
573 - Log_2 fold changes were calculated for each type of RNA.
574 - The total amount of validated sites each miRNA has on each circRNA (when present) was
575 added.

576 • A relative number of available sites per circRNA for each miRNA was determined by multiplying
577 the number of sites the miRNA has on a given circRNA by that circRNA's junction reads.
578 • By adding all the sites miRNAs have among circRNA (and their expression), a total amount of
579 available sites was calculated (referred to as 'effective' sites later on).
580 • A "sponging coefficient" was defined by taking the total amount of available sites of a certain
581 miRNA and dividing it for its expression (pre-differentiation).
582 • Two different sets of candidates were highlighted using different criteria:
583 o Most "sponged" microRNAs, according to the "sponging coefficient".
584 o Most "sponging" circRNAs, considering the number of sites each circRNA carries for all
585 miRNAs multiplied by the number of junction reads.
586 • All graphs were programmed and illustrated using ggplot2 package (Wickham, 2016), ggrepel
587 package (https://CRAN.R-project.org/package=ggrepel), hrbrthemes package
588 (https://CRAN.R-project.org/package=hrbrthemes) and/or viridis package (https://CRAN.R-
589 project.org/package=viridis), except for the network diagram (Figure S4A) which was done
590 using IGraph package (https://igraph.org/r/). Statistical analysis of the boxplots was done and
591 added to the graphs using ggsignif
592 (https://www.rdocumentation.org/packages/ggsignif/versions/0.6.1) and/or ggpubr
593 (https://rpkgs.datanovia.com/ggpubr/index.html).
594 • For pri-miRNA analysis we used the Galaxy platform (Afgan *et al*, 2018). Briefly, raw reads were
595 trimmed using Trim Galore! and mapped to the human reference genome (hg38) with the RNA-
596 STAR aligner (Dobin *et al*, 2013). Pri-miR counts were obtained from the mapped BAM files
597 using featureCounts (Liao *et al*, 2014) and the annotation file (has.gff3) retrieved from miRBase
598 (Kozomara *et al*, 2019).
599

600 **Bioinformatic analysis of miR-7 and miR-181b/d targets**

601 Targets for miR-7 were retrieved from TargetScan 7.1 mouse (Agarwal *et al*, 2015) while the ones for
602 miR-181b/d from TargetScan 7.2 human (Agarwal *et al*, 2015). Raw RNA-seq counts were downloaded
603 for CDR1as/ciRS-7 KO data (Piwecka *et al*, 2017) and circCSNK1G3 KD (Chen *et al*, 2019), accessions
604 GSE93130 and GSE113124, respectively. A differential expression analysis was done using the DESeq2

605 package (Love *et al*, 2014). Graphs were made using the results of the analysis and the packages
606 mentioned above.
607

608 Acknowledgements

609 We thank Isabel Roditi for providing materials and discussing experiments, Helge Grosshans and
610 Alberto R. Kornblihtt for a critical reading of the manuscript. M.d.l.M. is funded by grants from Agencia
611 Nacional de Promocion Cientifica y Tecnológica (ANPCyT) of Argentina (PICT- 2016-0499 and PICT-2018-
612 0478_PRH 2016-0002). D.R. acknowledges the support of the Volkswagen, Stiftung, the Max Planck
613 Society, the Fondo para la Convergencia Estructural de Mercosur (COF 03/11), the Agencia Nacional de
614 Promoción Científica y Tecnológica (ANPCyT) of Argentina (PICT- 2019-0499 and PICT-PRH 2014-3782)
615 and the Ministerio de Ciencia, Tecnología e Innovación Productiva of Argentina (MinCyT-BMBF
616 AL15/10). J.P.F. is funded by grants from Ministerio de Ciencia, Tecnología e Innovación Productiva of
617 Argentina (MINCyT) (BMBF/MINCYT MIGRAMIRNA Al/17/05), Agencia Nacional de Promocion Cientifica
618 y Tecnologica (ANPCyT) of Argentina (PICT-2017-2401, PCE-GSK-2017-0052), Glaxo-SmithKline (PCE-
619 GSK-2017-0052) and Fundación Progreso de la Medicina (GF N03/2017).
620

621 Author contributions

622 D.R. and M.d.l.M. conceived the project and designed and interpreted the experiments. F.F.W. and J.L.
623 designed, performed and interpreted most of the experiments. F.F.W. conceived, performed and
624 interpreted all bioinformatics analysis. J.L. and S.G. handled animals and prepared the neuron primary
625 cultures. L.B. performed the subcellular fractionation experiments. B.P. performed the northern blot
626 analysis. P.G. performed the subcloning of some of the constructs used in the study. J.P.F. designed
627 some of the experiments and discussed experimental strategies. D.R. and M.d.l.M. co-supervised the
628 whole project. The manuscript was written by F.F.W., D.R. and M.d.l.M.
629

630 Conflict of interest

631 The authors declare that they have no conflict of interest.

632 # References

633 Afgan E, Baker D, Batut B, van den Beek M, Bouvier D, Čech M, Chilton J, Clements D, Coraor N, Grüning
634 BA, *et al* (2018) The Galaxy platform for accessible, reproducible and collaborative biomedical
635 analyses: 2018 update. *Nucleic Acids Res* 46: W537–W544

636 Agarwal V, Bell GW, Nam JW & Bartel DP (2015) Predicting effective microRNA target sites in mammalian
637 mRNAs. *Elife* 4: 1–38

638 Ameres SL, Horwich MD, Hung J-H, Xu J, Ghildiyal M, Weng Z & Zamore PD (2010a) Target RNA-directed
639 trimming and tailing of small silencing RNAs. *Science* 328: 1534–9

640 Ameres SL, Horwich MD, Hung JH, Xu J, Ghildiyal M, Weng Z & Zamore PD (2010b) Target RNA-directed
641 trimming and tailing of small silencing RNAs. *Science (80-)* 328: 1534–1539

642 Ameres SL & Zamore PD (2013) Diversifying microRNA sequence and function. *Nat Rev Mol Cell Biol* 14:
643 475–488 doi:10.1038/nrm3611 [PREPRINT]

644 Bartel DP (2018) Metazoan MicroRNAs. *Cell* 173: 20–51

645 Bitetti A, Mallory AC, Golini E, Carrieri C, Carreño Gutiérrez H, Perlas E, Pérez-Rico YA, Tocchini-Valentini
646 GP, Enright AJ, Norton WHJ, *et al* (2018) MicroRNA degradation by a conserved target RNA
647 regulates animal behavior. *Nat Struct Mol Biol* 25: 244–251

648 Bosson AD, Zamudio JR & Sharp PA (2014) Endogenous miRNA and target concentrations determine
649 susceptibility to potential ceRNA competition. *Mol Cell* 56: 347–359

650 Brown BD, Gentner B, Cantore A, Colleoni S, Amendola M, Zingale A, Baccarini A, Lazzari G, Galli C &
651 Naldini L (2007) Endogenous microRNA can be broadly exploited to regulate transgene
652 expression according to tissue, lineage and differentiation state. *Nat Biotechnol* 25: 1457–1467

653 Cazalla D, Yario T, Steitz J a & Steitz J (2010a) Down-regulation of a host microRNA by a Herpesvirus
654 saimiri noncoding RNA. *Science* 328: 1563–6

655 Cazalla D, Yario T & Steitz JA (2010b) Down-regulation of a host microRNA by a Herpesvirus saimiri
656 noncoding RNA. *Science (80-)* 328: 1563–1566

657 Chen L (2020) The expanding regulatory mechanisms and cellular functions of circular RNAs. *Nat Rev*
658 *Mol Cell Biol* 21: 475–490

659 Chen S, Huang V, Xu X, Livingstone J, Soares F, Jeon J, Zeng Y, Hua JT, Petricca J, Guo H, *et al* (2019)
660 Widespread and Functional RNA Circularization in Localized Prostate Cancer. *Cell* 176: 831-

661 843.e22
662 Chen T, Xiang JF, Zhu S, Chen S, Yin QF, Zhang XO, Zhang J, Feng H, Dong R, Li XJ, *et al* (2015) ADAR1 is
663 required for differentiation and neural induction by regulating microRNA processing in a
664 catalytically independent manner. *Cell Res* 25: 459–476
665 Conn SJ, Pillman KA, Toubia J, Conn VM, Salmanidis M, Phillips CA, Roslan S, Schreiber AW, Gregory PA
666 & Goodall GJ (2015) The RNA binding protein quaking regulates formation of circRNAs. *Cell* 160:
667 1125–1134
668 de la Mata M, Gaidatzis D, Vitanescu M, Stadler MB, Wentzel C, Scheiffele P, Filipowicz W & Großhans H
669 (2015) Potent degradation of neuronal miRNAs induced by highly complementary targets. *EMBO*
670 *Rep* 16: 500–511
671 Denzler R, Agarwal V, Stefano J, Bartel DP & Stoffel M (2014) Assessing the ceRNA Hypothesis with
672 Quantitative Measurements of miRNA and Target Abundance. *Mol Cell* 54: 766–776
673 Denzler R, McGeary SE, Title AC, Agarwal V, Bartel DP & Stoffel M (2016) Impact of MicroRNA Levels,
674 Target-Site Complementarity, and Cooperativity on Competing Endogenous RNA-Regulated
675 Gene Expression. *Mol Cell* 64: 565–579
676 Dobin A, Davis CA, Schlesinger F, Drenkow J, Zaleski C, Jha S, Batut P, Chaisson M & Gingeras TR (2013)
677 STAR: ultrafast universal RNA-seq aligner. *Bioinformatics* 29: 15–21
678 Dodbele S, Mutlu N & Wilusz JE (2021) Best practices to ensure robust investigation of circular RNAs:
679 pitfalls and tips. *EMBO Rep* 22: 1–12
680 Fellmann C, Hoffmann T, Sridhar V, Hopfgartner B, Muhar M, Roth M, Lai DY, Barbosa IAM, Kwon JS, Guan
681 Y, *et al* (2013) An optimized microRNA backbone for effective single-copy RNAi. *Cell Rep*
682 Fuchs Wightman F, Giono LE, Fededa JP & de la Mata M (2018) Target RNAs Strike Back on MicroRNAs.
683 *Front Genet* 9
684 Gascón S, Paez-Gomez JA, Díaz-Guerra M, Scheiffele P & Scholl FG (2008) Dual-promoter lentiviral
685 vectors for constitutive and regulated gene expression in neurons. *J Neurosci Methods*
686 Gasparini S, Licursi V, Presutti C & Mannironi C (2020) The Secret Garden of Neuronal circRNAs. *Cells* 9:
687 1815
688 Ghini F, Rubolino C, Climent M, Simeone I, Marzi MJ & Nicassio F (2018) Endogenous transcripts control
689 miRNA levels and activity in mammalian cells by target-directed miRNA degradation. *Nat*

690 *Commun* 9: 3119
691 Gibson DG, Young L, Chuang R-Y, Venter JC, Hutchison CA & Smith HO (2009) Enzymatic assembly of
692 DNA molecules up to several hundred kilobases. *Nat Methods* 6: 343–345
693 Giusti SA, Vogl AM, Brockmann MM, Vercelli CA, Rein ML, Trumbach D, Wurst W, Cazalla D, Stein V,
694 Deussing JM, *et al* (2014) MicroRNA-9 controls dendritic development by targeting REST. *Elife* 3
695 Guarnerio J, Zhang Y, Cheloni G, Panella R, Mae Katon J, Simpson M, Matsumoto A, Papa A, Loretelli C,
696 Petri A, *et al* (2019) Intragenic antagonistic roles of protein and circRNA in tumorigenesis. *Cell Res*
697 29: 628–640
698 Han J, Han J, Lavigne CA, Jones BT, Zhang H, Gillett F & Mendell JT (2020) A ubiquitin ligase mediates
699 target-directed microRNA decay independently of tailing and trimming. *Science (80-)* 9546: 1–17
700 Hanan M, Simchovitz A, Yayon N, Vaknine S, Cohen-Fultheim R, Karmon M, Madrer N, Rohrlich TM,
701 Maman M, Bennett ER, *et al* (2020) A Parkinson's disease CircRNAs Resource reveals a link between
702 circSLC8A1 and oxidative stress. *EMBO Mol Med*: e11942
703 Hansen TB, Jensen TI, Clausen BH, Bramsen JB, Finsen B, Damgaard CK & Kjems J (2013) Natural RNA
704 circles function as efficient microRNA sponges. *Nature* 495: 384–388
705 Hansen TB, Wiklund ED, Bramsen JB, Villadsen SB, Statham AL, Clark SJ & Kjems J (2011) miRNA-
706 dependent gene silencing involving Ago2-mediated cleavage of a circular antisense RNA. *EMBO J*
707 30: 4414–4422
708 Jeck WR, Sorrentino JA, Wang K, Slevin MK, Burd CE, Liu J, Marzluff WF & Sharpless NE (2013) Circular
709 RNAs are abundant, conserved, and associated with ALU repeats. *RNA* 19: 141–157
710 Jens M & Rajewsky N (2015) Competition between target sites of regulators shapes post-transcriptional
711 gene regulation. *Nat Rev Genet* 16: 113–126
712 Jonas S & Izaurralde E (2015) Towards a molecular understanding of microRNA-mediated gene
713 silencing. *Nat Rev Genet* 16: 421–433
714 Kleaveland B, Shi CY, Stefano J & Bartel DP (2018) A Network of Noncoding Regulatory RNAs Acts in the
715 Mammalian Brain. *Cell* 174: 350-362.e17
716 Kozomara A, Birgaoanu M & Griffiths-Jones S (2019) miRBase: from microRNA sequences to function.
717 *Nucleic Acids Res* 47: D155–D162
718 Kramer MC, Liang D, Tatomer DC, Gold B, March ZM, Cherry S & Wilusz JE (2015) Combinatorial control

719 of Drosophila circular RNA expression by intronic repeats, hnRNPs, and SR proteins. *Genes Dev* 29:
720 2168–2182
721 Kristensen LS, Andersen MS, Stagsted LVW, Ebbesen KK, Hansen TB & Kjems J (2019) The biogenesis,
722 biology and characterization of circular RNAs. *Nat Rev Genet* 20: 675–691
723 Krol J, Busskamp V, Markiewicz I, Stadler MB, Ribi S, Richter J, Duebel J, Bicker S, Fehling HJJ, Schubeler
724 D, *et al* (2010) Characterizing light-regulated retinal microRNAs reveals rapid turnover as a
725 common property of neuronal microRNAs. *Cell* 141: 618–631
726 Lee S, Song J, Kim S, Kim J, Hong Y, Kim Y & Kim D (2013) Selective Degradation of Host MicroRNAs by
727 an Intergenic HCMV Noncoding RNA Accelerates Virus Production. *Cell Host Microbe* 13: 678–690
728 Li JH, Liu S, Zhou H, Qu LH & Yang JH (2014) StarBase v2.0: Decoding miRNA-ceRNA, miRNA-ncRNA and
729 protein-RNA interaction networks from large-scale CLIP-Seq data. *Nucleic Acids Res*
730 Li L, Sheng P, Li T, Fields CJ, Hiers NM, Wang Y, Li J, Guardia CM, Licht JD & Xie M (2021) Widespread
731 microRNA degradation elements in target mRNAs can assist the encoded proteins. *Genes Dev* 35
732 Li X, Liu CX, Xue W, Zhang Y, Jiang S, Yin QF, Wei J, Yao RW, Yang L & Chen LL (2017) Coordinated circRNA
733 Biogenesis and Function with NF90/NF110 in Viral Infection. *Mol Cell* 67: 214-227.e7
734 Liang D & Wilusz JE (2014) Short intronic repeat sequences facilitate circular RNA production. *Genes Dev*
735 28: 2233–2247
736 Liao Y, Smyth GK & Shi W (2014) featureCounts: an efficient general purpose program for assigning
737 sequence reads to genomic features. *Bioinformatics* 30: 923–930
738 Litke JL & Jaffrey SR (2019) Highly efficient expression of circular RNA aptamers in cells using
739 autocatalytic transcripts. *Nat Biotechnol* 37: 667–675
740 Liu CX, Li X, Nan F, Jiang S, Gao X, Guo SK, Xue W, Cui Y, Dong K, Ding H, *et al* (2019) Structure and
741 Degradation of Circular RNAs Regulate PKR Activation in Innate Immunity. *Cell* 177: 865-880.e21
742 Love MI, Huber W & Anders S (2014) Moderated estimation of fold change and dispersion for RNA-seq
743 data with DESeq2. *Genome Biol*
744 Marcinowski L, Tanguy M, Krmpotic A, Rädle B, Lisnić VJ, Tuddenham L, Chane-Woon-Ming B, Ruzsics Z,
745 Erhard F, Benkartek C, *et al* (2012) Degradation of cellular miR-27 by a novel, highly abundant viral
746 transcript is important for efficient virus replication in vivo. *PLoS Pathog* 8
747 Memczak S, Jens M, Elefsinioti A, Torti F, Krueger J, Rybak A, Maier L, Mackowiak SD, Gregersen LH,

Munschauer M, *et al* (2013) Circular RNAs are a large class of animal RNAs with regulatory potency. *Nature* 495: 333–338

Pamudurti NR, Bartok O, Jens M, Ashwal-Fluss R, Stottmeister C, Ruhe L, Hanan M, Wyler E, Perez-Hernandez D, Ramberger E, *et al* (2017) Translation of CircRNAs. *Mol Cell* 66: 9-21.e7

Pawlica P, Moss WN & Steitz JA (2016) Host miRNA degradation by Herpesvirus saimiri small nuclear RNA requires an unstructured interacting region. *RNA* 22: 1181–1189

Petkovic S, Graff S, Feller N, Berghaus J, Ruppert V-P, Dülfer J & Sczakiel G (2021) Circular versus linear RNA topology: different modes of RNA-RNA interactions in vitro and in human cells. *RNA Biol*: 1–10

Pinzon N, Li B, Martinez L, Sergeeva A, Presumey J, Apparailly F & Seitz H (2017) microRNA target prediction programs predict many false positives. *Genome Res* 27: 234–245

Piwecka M, Glažar P, Hernandez-Miranda LR, Memczak S, Wolf SA, Rybak-Wolf A, Filipchyk A, Klironomos F, Cerda Jara CA, Fenske P, *et al* (2017) Loss of a mammalian circular RNA locus causes miRNA deregulation and affects brain function. *Science (80-)* 8526: eaam8526

Roditi I, Carrington M & Turner M (1987) Expression of a polypeptide containing a dipeptide repeat is confined to the insect stage of Trypanosoma brucei. *Nature* 325: 272–274

Rybak-Wolf A, Stottmeister C, Glažar P, Jens M, Pino N, Hanan M, Behm M, Bartok O, Ashwal-Fluss R, Herzog M, *et al* (2015) Circular RNAs in the Mammalian Brain Are Highly Abundant, Conserved, and Dynamically Expressed. *Mol Cell* 58: 870–885

Salzman J, Chen RE, Olsen MN, Wang PL & Brown PO (2013) Cell-type specific features of circular RNA expression. *PLoS Genet* 9: e1003777

Sanjana NE, Shalem O & Zhang F (2014) Improved vectors and genome-wide libraries for CRISPR screening. *Nat Methods* doi:10.1038/nmeth.3047 [PREPRINT]

Shalem O, Sanjana NE, Hartenian E, Shi X, Scott DA, Mikkelsen TS, Heckl D, Ebert BL, Root DE, Doench JG, *et al* (2014) Genome-scale CRISPR-Cas9 knockout screening in human cells. *Science (80-)*

Shi CY, Kingston ER, Kleaveland B, Lin DH, Stubna MW & Bartel DP (2020) The ZSWIM8 ubiquitin ligase mediates target-directed microRNA degradation. *Science (80-)* 370: eabc9359

Simeone I, Rubolino C, Noviello TMR, Farinello D, Cerulo L, Marzi MJ & Nicassio F (2022) Prediction and pan-cancer analysis of mammalian transcripts involved in target directed miRNA degradation.

Nucleic Acids Res 50: 2019–2035

Tay Y, Rinn J & Pandolfi PP (2014) The multilayered complexity of ceRNA crosstalk and competition. *Nature* 505: 344–352

Vogl AM, Brockmann MM, Giusti SA, Maccarrone G, Vercelli CA, Bauder CA, Richter JS, Roselli F, Hafner AS, Dedic N, *et al* (2015) Neddylation inhibition impairs spine development, destabilizes synapses and deteriorates cognition. *Nat Neurosci* 18: 239–251

Wickham H (2016) ggplot2: Elegant Graphics for Data Analysis Springer-Verlag New York

Wickham H, Averick M, Bryan J, Chang W, McGowan L, François R, Grolemund G, Hayes A, Henry L, Hester J, *et al* (2019) Welcome to the Tidyverse. *J Open Source Softw*

Xiao MS, Ai Y & Wilusz JE (2020) Biogenesis and Functions of Circular RNAs Come into Focus. *Trends Cell Biol* doi:10.1016/j.tcb.2019.12.004 [PREPRINT]

Yang JH, Li JH, Shao P, Zhou H, Chen YQ & Qu LH (2011) StarBase: A database for exploring microRNA-mRNA interaction maps from Argonaute CLIP-Seq and Degradome-Seq data. *Nucleic Acids Res*

You X, Vlatkovic I, Babic A, Will T, Epstein I, Tushev G, Akbalik GGG, Wang M, Glock C, Quedenau C, *et al* (2015) Neural circular RNAs are derived from synaptic genes and regulated by development and plasticity. *Nat Neurosci* 18: 603–610

Zhang XO, Wang H Bin, Zhang Y, Lu X, Chen LL & Yang L (2014) Complementary sequence-mediated exon circularization. *Cell* 159: 134–147

Zhang Y, Xue W, Li X, Zhang J, Chen S, Zhang JL, Yang L & Chen LL (2016) The Biogenesis of Nascent Circular RNAs. *Cell Rep* 15: 611–624

799 # Figure legends

800 **Figure 1.**

801 System to artificially express circRNAs free of their overlapping, cognate linear RNA.

802 (A) Top: Illustration of the linear RNA expressing construct used as a positive control for TDMD
803 Bottom: Illustration of the circRNA expressing construct. Depicted with coloured arrows are the
804 sets of primers used to measure the different transcript variants (circular [1], Total Output-TO [2]
805 and linear [3]).

806 (B) Total output, Linear and circular RNA levels upon expression of the artificial circRNA constructs
807 from the tetracycline-inducible promoter (TREp) bearing perfectly matched or seed-mutant miR-
808 124 sites for selective linear RNA degradation (see Figure S1A).

809 (C) Total output (left) and circRNA levels (right) upon expression of the artificial circRNA construct
810 versus the linear RNA construct (TDMD inducer). The constructs were expressed from the
811 tetracycline-inducible promoter (TREp) and the synapsin (Syn) promoter respectively in order to
812 achieve similar Total output levels for both constructs. Error bars represent the standard error of
813 the mean (SEM). Statistical significance was determined by unpaired *t* tests (ns: $p > 0.05$, *: $p <= 0.05$,
814 **: $p <= 0.01$, ***: $p <= 0.001$, ****: $p <= 0.0001$).

815

816 **Figure 2.**

817 Artificial circRNAs are unable to trigger TDMD.

818 (A) MiR-132 levels upon expression of linear (left) or circular (right) RNAs carrying bulged (TDMD-
819 competent) or seed-mutant miR-132 sites.

820 (B) AGO2-Flag immunoprecipitation (RIP) followed by RT-qPCR in HEK293T cells. MiR-27a was used
821 to normalize expression (RT-qPCR/Taqman assay). CircRNA expression was measured using
822 circRNA-backspliced-junction specific divergent primers and normalized to miR-27a levels (RT-
823 qPCR/Taqman assay) as an unrelated RISC-loaded miRNA not expected to be affected by the
824 circRNA. Non-specific U6 background binding to Ago2 is shown. As an IP quality control,
825 FLAG/HA-AGO2 input levels were shown to be similar across conditions and efficiently pulled-
826 down using anti-FLAG beads (Figure S2A). Accordingly, miR-27, but not U6 RNA, was efficiently
827 co-immunoprecipitated (Figure S2B).

828 (C) Subcellular fractionation showing total vs. cytoplasmic (left) and total vs. nuclear (right) fractions,
829 followed by RT-qPCR of the circRNA and linear RNA isoforms, normalized by Gapdh (for
830 cytoplasm) or U6 (for nucleus). Fractionation efficiency was assessed via Western Blot and RT-
831 qPCR (Figure S2C-D). Error bars represent the standard error of the mean (SEM). Statistical
832 significance was determined by unpaired *t* tests (ns: p > 0.05, *: p <= 0.05, **: p <= 0.01, ***: p <=
833 0.001, ****: p <= 0.0001).
834
835 **Figure 3.**
836 Endogenous CDR1as/ciRS-7 lacks TDMD activity on miR-7.
837 (A) Left: CDR1as/ciRS-7 total output (linear plus circular) levels measured by RT-qPCR upon
838 coinfection of either a scrambled shRNA or shCDR1as alone or shCDR1as rescued with a linear
839 version of linCDR1as lacking the shCDR1as site, in mouse cortex primary neurons. Right: MiR-7
840 levels measured by Taqman RT-qPCR upon coinfection of either a scrambled shRNA or shCDR1as
841 alone or shCDR1as rescued with a linear version of linCDR1as lacking the shCDR1as site, in mouse
842 cortex primary neurons.
843 (B) Left: CDR1as/ciRS-7 total output levels upon over-expression of linear CDR1as/ciRS-7
844 (linCDR1as), measured by RT-qPCR, in hippocampal primary neurons. Right: Circular
845 CDR1as/ciRS-7 level upon over-expression of linear CDR1as/ciRS-7, measured by RT-qPCR, in
846 hippocampal primary neurons.
847 (C) MiR-7 targets levels upon over-expression of linear CDR1as/ciRS-7 measured by RT-qPCR, in
848 hippocampal primary neurons.
849 (D-E) Re-analyzed data from Piwecka et al. 2017 (Piwecka *et al*, 2017). Shown are mRNA fold changes
850 in cortex neurons of CDR1as/ciRS-7 KO vs. WT mice.
851 (D) Volcano plot of genes predicted as not targeted by miR-7 are depicted in grey and miR-7
852 predicted targets in red (p-Adj > 0.05) or blue (p-Adj < 0.05).
853 (E) Box plot displaying an overall upregulation of predicted miR-7 targets upon CDR1as/ciRS-7
854 KO.
855 Error bars represent the standard error of the mean (SEM). Statistical significance was determined by
856 unpaired *t* tests (ns: p > 0.05, *: p <= 0.05, **: p <= 0.01, ***: p <= 0.001, ****: p <= 0.0001).

857

858 **Figure 4.**

859 CircRNAs potentially stabilize dozens of microRNAs along neuron-like differentiation.

860 (A) miRNA expression fold changes across differentiation. Plotted are fold changes (log2) in miRNA
861 levels across differentiation versus the expression (RPM) pre-differentiation, coloured by the
862 amount of 'effective' sites in circRNAs.

863 (B-C) The predicted most highly 'sponged' miRNAs show the highest fold changes across
864 differentiation. Plotted are fold changes (log2) in miRNA levels versus their 'sponging' coefficient
865 score (log10) coloured by quartiles in scatter plot (B) or as a boxplot. Unpaired t-tests are shown
866 between the most sponged and the remaining groups (ns: $p > 0.05$, *: $p <= 0.05$, **: $p <= 0.01$,
867 ***: $p <= 0.001$, ****: $p <= 0.0001$).

868 (D) Transcription rates does not account for the larger fold change across differentiation observed
869 for the most highly 'sponged' miRNAs. Pri-miRNA levels were taken as a proxy for transcription
870 rates. Scatterplots faceted by 'sponging' coefficient quartiles. Plotted are the fold change (log2)
871 of the miRNAs versus the pri-miR fold change (log2).

872 (E) circRNA expression fold changes across differentiation. Plotted are the fold changes (log2) in
873 circRNA levels versus the expression (junction reads) pre-differentiation, coloured by the number
874 of 'effective' sites each circRNA has for all miRNAs.

875 (F) Increasing number of predicted miRNA binding sites does not affect circRNAs levels. Boxplot
876 show the fold change (log2) across differentiation of circRNAs with increasing miRNA sites.

877

878 **Figure S1.**

879 Artificial circRNA constructs and quality controls.

880 (A) Table summarizing the constructs generated.

881 (B) circRNAs are resistant to RNase R digestion, confirming the circular topology of the artificial
882 circRNA. RNase R treated samples from Primary Neurons or HEK293T cells were analyzed by RT-
883 qPCR using divergent primers (primers 1 of Fig. 1) amplifying across the backspliced junction to
884 measure levels of artificial circRNA or regular convergent primers (primers 2 and 3 in Fig 1) to
885 measure levels of total reporter output and cognate linear RNA, respectively.

886 (C) Top: Agarose gel showing triplicates of the qPCR amplicons obtained with divergent primers
887 against the backsplicing junction of the artificial circRNA, after retro-transcription with two
888 different reverse transcriptases (MMLV-RT & Superscript II) to rule out artifacts due to template
889 switching during cDNA synthesis. Bottom: Sanger sequencing of the amplicons shown above
890 confirming backsplicing junction in HEK293 cells.
891 (D) Northern blot analysis of RNase R treated or untreated samples from HEK293T cells expressing
892 the indicated artificial circRNA constructs. All constructs were expressed from the tetracycline-
893 inducible promoter (TREp). The asterisk (*) marks a putative mechanically linearized product of
894 the corresponding circRNA.
895 (E) Quantification by different methods of the linear and circular isoforms from RNase R untreated
896 samples of HEK293T cells (naturally lacking miR132) expressing the indicated constructs. Top
897 panels: digital densitometry quantification of Northern blot bands by ImageJ. Bottom panels: RT-
898 qPCR quantification using primers specific for the circular isoform or for both the linear and
899 circular isoforms combined (Total Output) depicted in Figure 1A. Note that HEK293T cells are
900 devoid of miR132.
901
902 **Figure S2.**
903 HA-FLAG/AGO2 RIP and cellular fractionation quality controls.
904 (A) Anti HA Western Blot in non-transfected cells or cells transfected with the artificial circRNA
905 bearing bulged (WT) or seed-mutant (mut) miR-132 sites.
906 (B) U6 and miR-27 levels were measured to corroborate the efficiency of HA-FLAG/AGO2
907 immunoprecipitation. Error bars represent the standard error of the mean (SEM). Statistical
908 significance was determined by unpaired *t* tests (ns: $p > 0.05$, *: $p <= 0.05$, **: $p <= 0.01$, ***: $p <=$
909 0.001, ****: $p <= 0.0001$).
910 (C) Western Blot showing cells transfected with either the artificial circRNA or the linear control RNA,
911 following subcellular fractionation. α-Tubulin and Histone-3 were used as cytoplasm and
912 nucleus markers, respectively.
913 (D) GAPDH/U6 ratio measured by RT-qPCR confirmed proper of subcellular fractionation of samples
914 either transfected with the artificial circRNA or the linear control. Statistical significance was

915 determined by a paired *t* test (ns: p > 0.05, *: p <= 0.05, **: p <= 0.01, ***: p <= 0.001, ****: p <=
916 0.0001).
917
918 **Figure S3.**
919 (A) Five examples of potential TDMD-competent binding sites for miR-7 present in CDR1as/ciRS-7.
920 (B) Endogenous circular CDR1as/ciRS-7 normalized levels upon over-expression of the linear version
921 of CDR1as/ciRS-7.
922 (C) Illustration of sgRNAs designed to edit CDR1as/ciRS-7 splicing cites by CRISPR/Cas9.
923 (D-E) CDR1as/ciRS-7 (D) and miR-7 (E) fold changes measured by RT-qPCR upon CRISPR/Cas9 editing
924 of CDR1as/ciRS-7 splicing site in mouse primary neurons.
925 (F) Illustration of the primer pair designs for measuring the different CDR1as/ciRS-7 isoforms
926 (detailed in Materials and Methods).
927 (G-H) Re-analyzed data from (Chen *et al*, 2019). Shown are mRNA fold changes in circCSNK1G3 KD vs.
928 WT PC-3 prostate cancer cell line. (G) Volcano plot of genes predicted as not targeted by miR-
929 181b/d are depicted in grey and miR-181b/d predicted targets in red (p-Adj > 0.05) or blue (p-
930 Adj < 0.05). (H) Box plot displaying an overall upregulation of predicted miR-181b/d targets upon
931 circCSNK1G3 KD.
932 Error bars represent the standard error of the mean (SEM). Statistical significance was determined by
933 unpaired *t* tests (ns: p > 0.05, *: p <= 0.05, **: p <= 0.01, ***: p <= 0.001, ****: p <= 0.0001). For the (D-E)
934 panels, equal variance was assumed.
935
936 **Figure S4.**
937 (A) Network diagram depicting biochemically validated interactions between circRNAs (the seven
938 'most sponging') and the miRNAs they interact with.
939 (B) Model of the protection effect of CDR1as/ciRS-7 on miR-7.

Figure 1

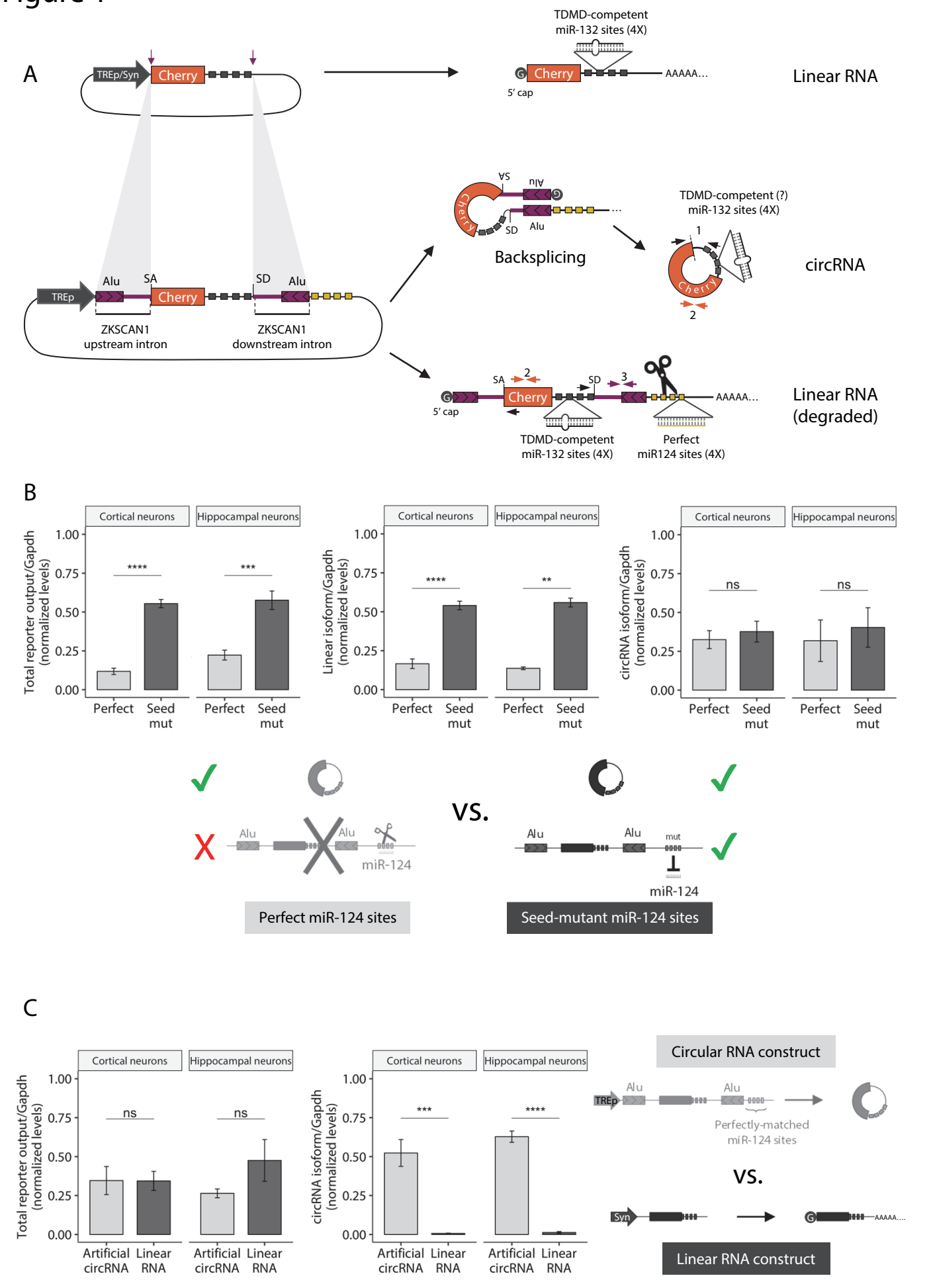
A
TREp/Syn
Cherry
TDMD-competent
miR-132 sites (4X)
5' cap
AAAAA...
Linear RNA
Alu
SA
SD
Backsplicing
TDMD-competent (?)
miR-132 sites (4X)
circRNA
TREp
ZKSCAN1
upstream intron
ZKSCAN1
downstream intron
Linear RNA
(degraded)
TDMD-competent
miR-132 sites (4X)
Perfect
miR124 sites (4X)
B
Cortical neurons
Hippocampal neurons
Total reporter output/Gapdh
(normalized levels)
Linear isoform/Gapdh
(normalized levels)
circRNA isoform/Gapdh
(normalized levels)
Perfect
Seed
mut
ns
VS.
miR-124
mut
Perfect miR-124 sites
Seed-mutant miR-124 sites
C
Artificial
circRNA
Linear
RNA
Circular RNA construct
Perfectly-matched
miR-124 sites
Syn
Linear RNA construct

Figure 2

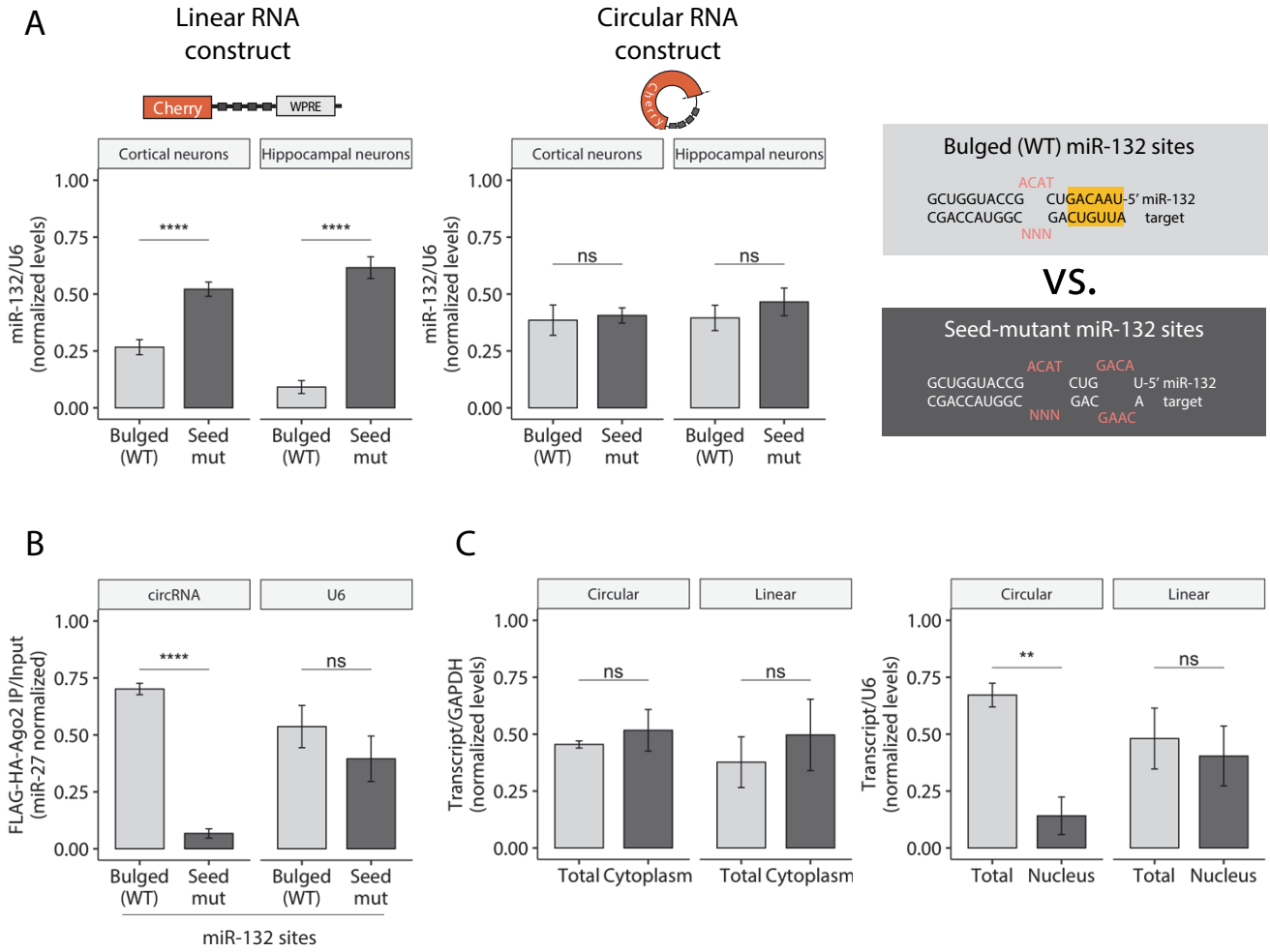
A
Linear RNA construct
Circular RNA construct
Cherry
WPRE
Cortical neurons
Hippocampal neurons
miR-132/U6 (normalized levels)
****
ns
Bulged (WT)
Seed mut
Bulged (WT) miR-132 sites
ACAT
GCUGGUACCG
CGACCAUGGC
CUGACAAU-5′ miR-132
GACUGUUA target
NNN
VS.
Seed-mutant miR-132 sites
ACAT
GACA
GCUGGUACCG
CGACCAUGGC
CUG
GAC
U-5′ miR-132
A target
NNN
GAAC
B
circRNA
U6
FLAG-HA-Ago2 IP/Input (miR-27 normalized)
miR-132 sites
C
Circular
Linear
Transcript/GAPDH (normalized levels)
Total
Cytoplasm
Transcript/U6 (normalized levels)
Nucleus
**

Figure 3

A

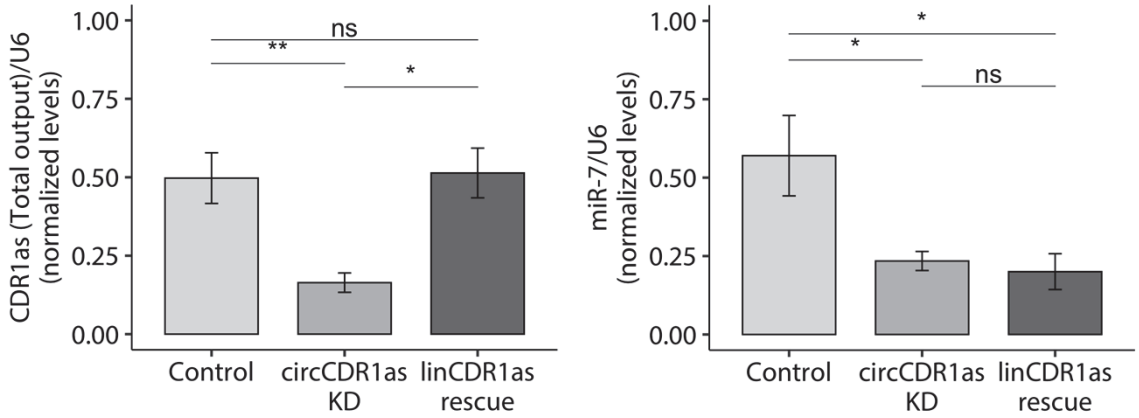

B

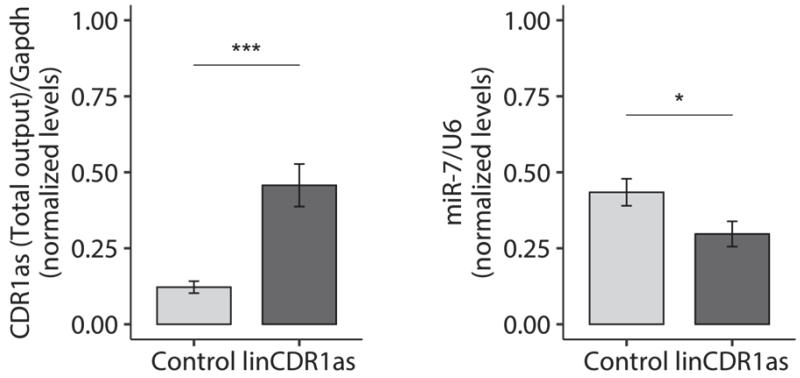

C

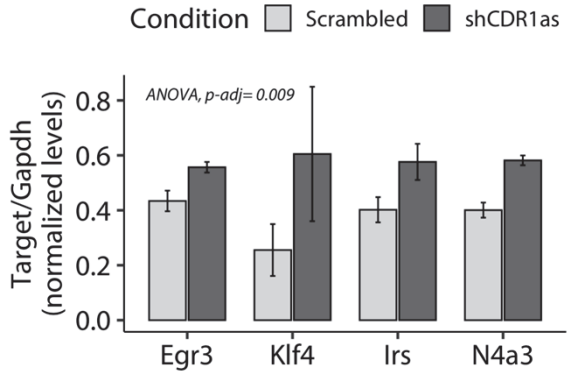

D

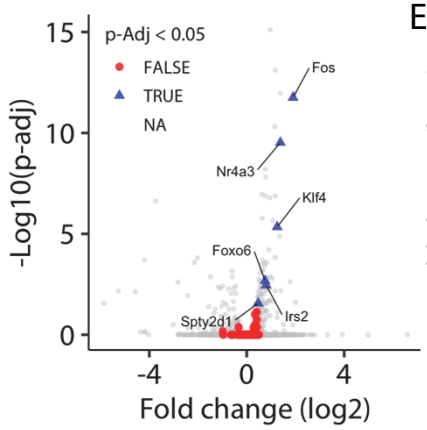

E

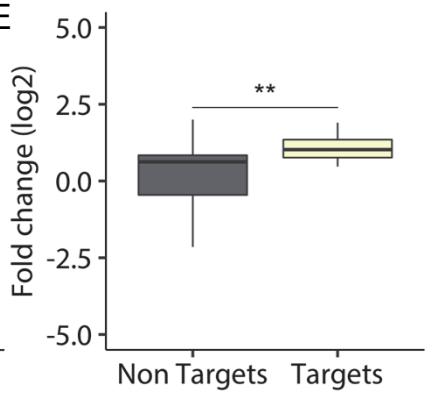

Figure 4

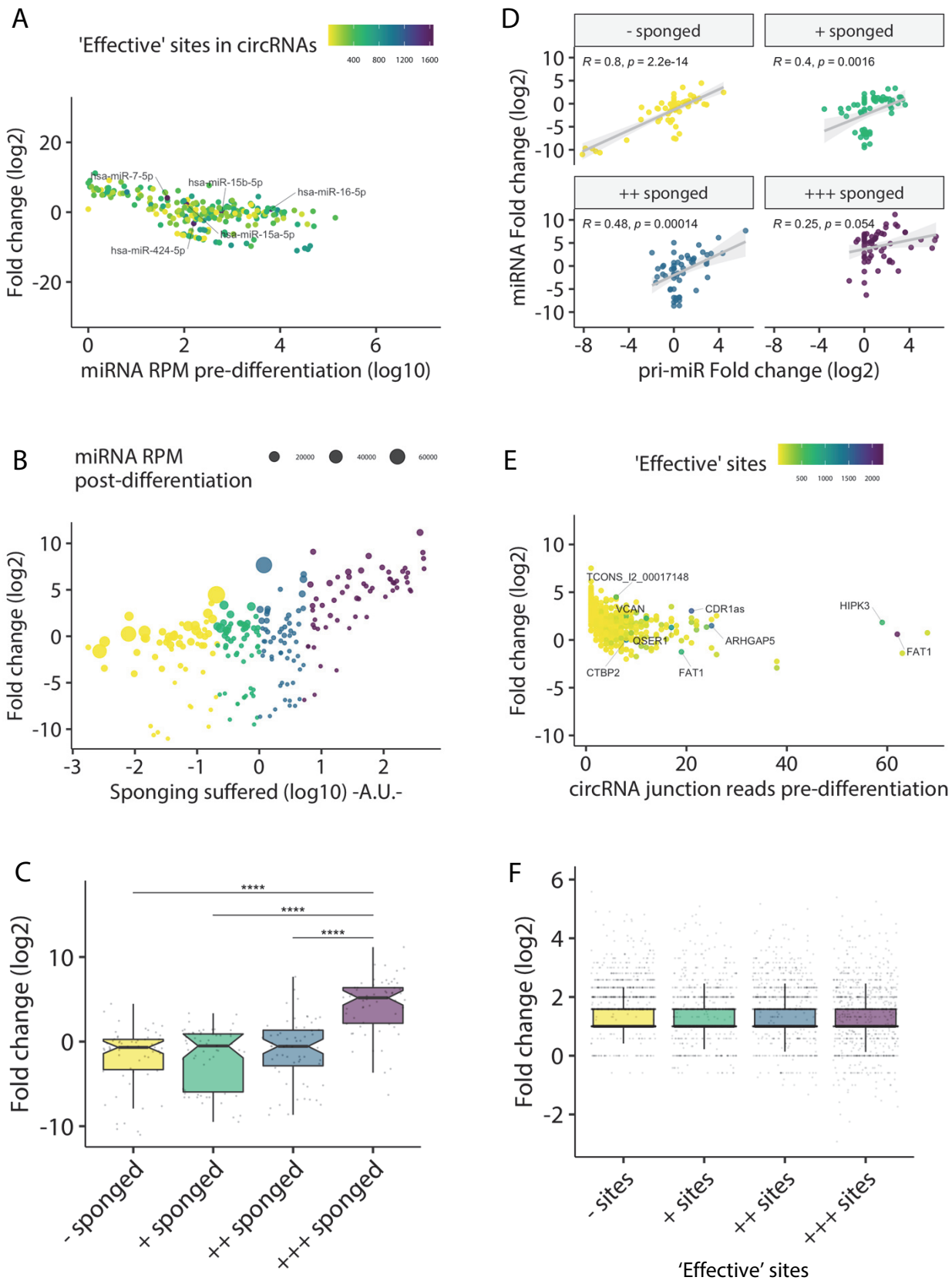
A
'Effective' sites in circRNAs
400 800 1200 1600
Fold change (log2)
hsa-miR-7-5p
hsa-miR-15b-5p
hsa-miR-16-5p
hsa-miR-15a-5p
hsa-miR-424-5p
miRNA RPM pre-differentiation (log10)
B
miRNA RPM post-differentiation
20000 40000 60000
Fold change (log2)
Sponging suffered (log10) -A.U.-
C
****
****
****
Fold change (log2)
- sponged
+ sponged
++ sponged
+++ sponged
D
- sponged
+ sponged
++ sponged
+++ sponged
R = 0.8, p = 2.2e-14
R = 0.4, p = 0.0016
R = 0.48, p = 0.00014
R = 0.25, p = 0.054
miRNA Fold change (log2)
pri-miR Fold change (log2)
E
'Effective' sites
500 1000 1500 2000
Fold change (log2)
TCONS_l2_00017148
VCAN
CDR1as
HIPK3
QSER1
ARHGAP5
FAT1
CTBP2
FAT1
circRNA junction reads pre-differentiation
F
Fold change (log2)
- sites
+ sites
++ sites
+++ sites
'Effective' sites

Figure S1

A

Construct purpose	TDMD-inducing sites (miR-132) Type	TDMD-inducing sites (miR-132) Architecture	Linear RNA targeting sites (miR-124) Type	Linear RNA targeting sites (miR-124) Architecture	Expected RNA topology
circRNA expression (linear RNA-depleted)	Bulged (WT)	GCUGGUACCG ACAT CUGACAAU-5′ miR-132 CGACCAUGGC NNN GACUGUUA target	Perfect match	CCGUAAGUGGCGCACGGAAU-5′ miR-124 GGCAUUCACCGCGUGCCUUA target	Circular
	Seed-mut	GCUGGUACCG ACAT CUG GACA U-5′ miR-132 CGACCAUGGC NNN GAC GAAC A target	Perfect match	CCGUAAGUGGCGCACGGAAU-5′ miR-124 GGCAUUCACCGCGUGCCUUA target	Circular
circRNA expression (control)	Bulged (WT)	GCUGGUACCG ACAT CUGACAAU-5′ miR-132 CGACCAUGGC NNN GACUGUUA target	Seed-mut	CCGUAAGU GGCG CA CGGA AU-5′ miR-124 GGCAUUCA NNN GU CGGA UA target	Circular + linear leak
	Seed-mut	GCUGGUACCG ACAT CUG GACA U-5′ miR-132 CGACCAUGGC NNN GAC GAAC A target	Seed-mut	CCGUAAGU GGCG CA CGGA AU-5′ miR-124 GGCAUUCA NNN GU CGGA UA target	Circular + linear leak
linear RNA expression (TDMD positive control)	Bulged (WT)	GCUGGUACCG ACAT CUGACAAU-5′ miR-132 CGACCAUGGC NNN GACUGUUA target	NA	NA	Linear
	Seed-mut	GCUGGUACCG ACAT CUG GACA U-5′ miR-132 CGACCAUGGC NNN GAC GAAC A target	NA	NA	Linear

B

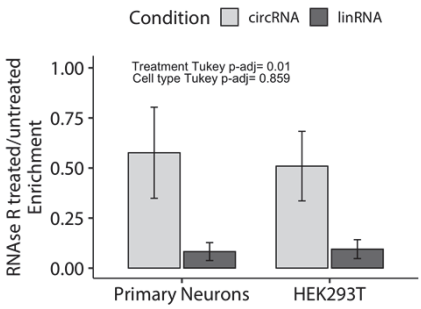

C

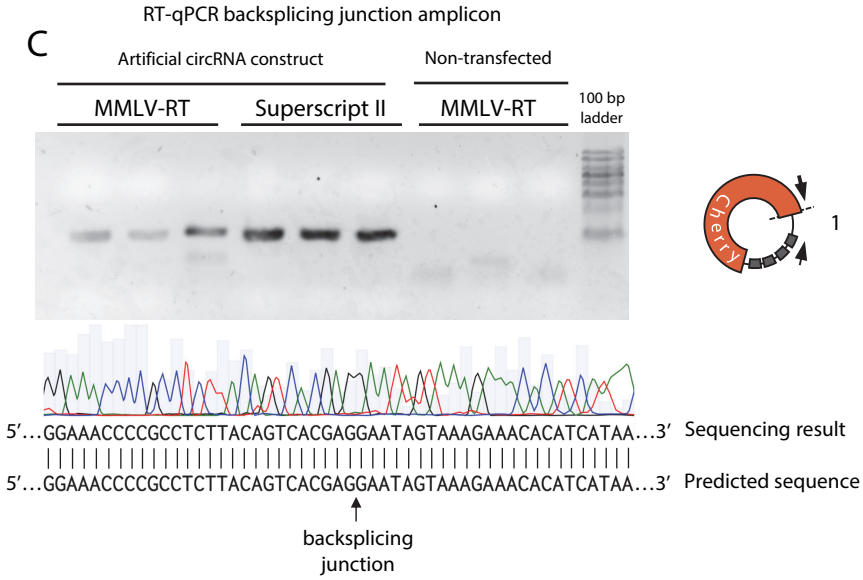

D

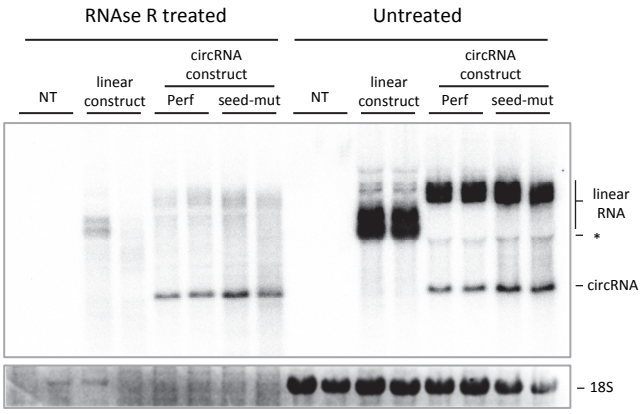

E

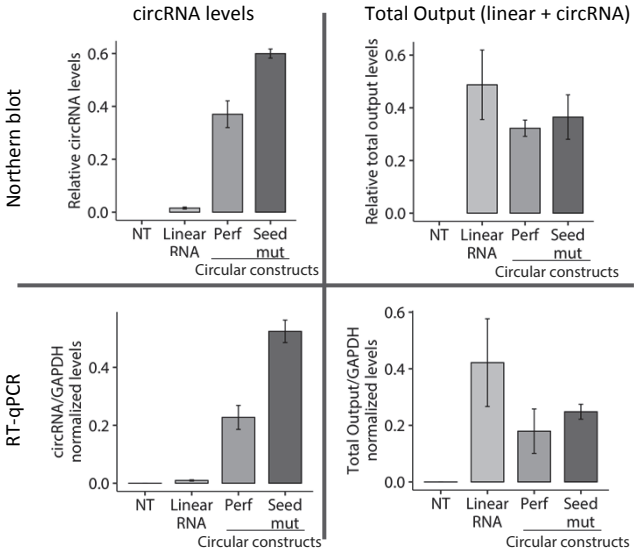

Figure S2

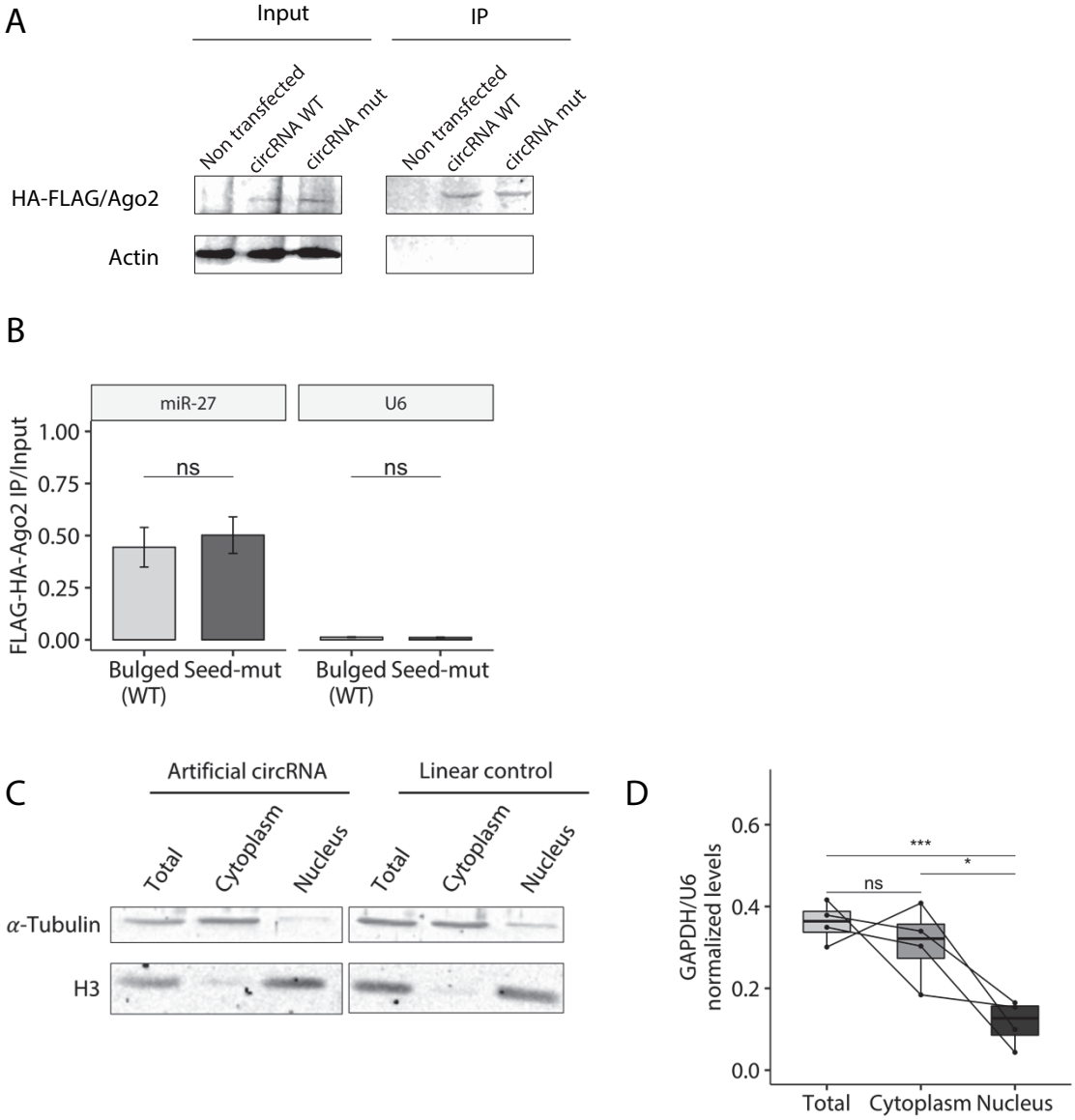
A
Input
IP
Non transfected
circRNA WT
circRNA mut
Non transfected
circRNA WT
circRNA mut
HA-FLAG/Ago2
Actin
B
miR-27
U6
FLAG-HA-Ago2 IP/Input
1.00
0.75
0.50
0.25
0.00
ns
ns
Bulged (WT)
Seed-mut
Bulged (WT)
Seed-mut
C
Artificial circRNA
Linear control
Total
Cytoplasm
Nucleus
Total
Cytoplasm
Nucleus
α-Tubulin
H3
D
GAPDH/U6 normalized levels
0.6
0.4
0.2
0.0
***
*
ns
Total
Cytoplasm
Nucleus

Figure S3

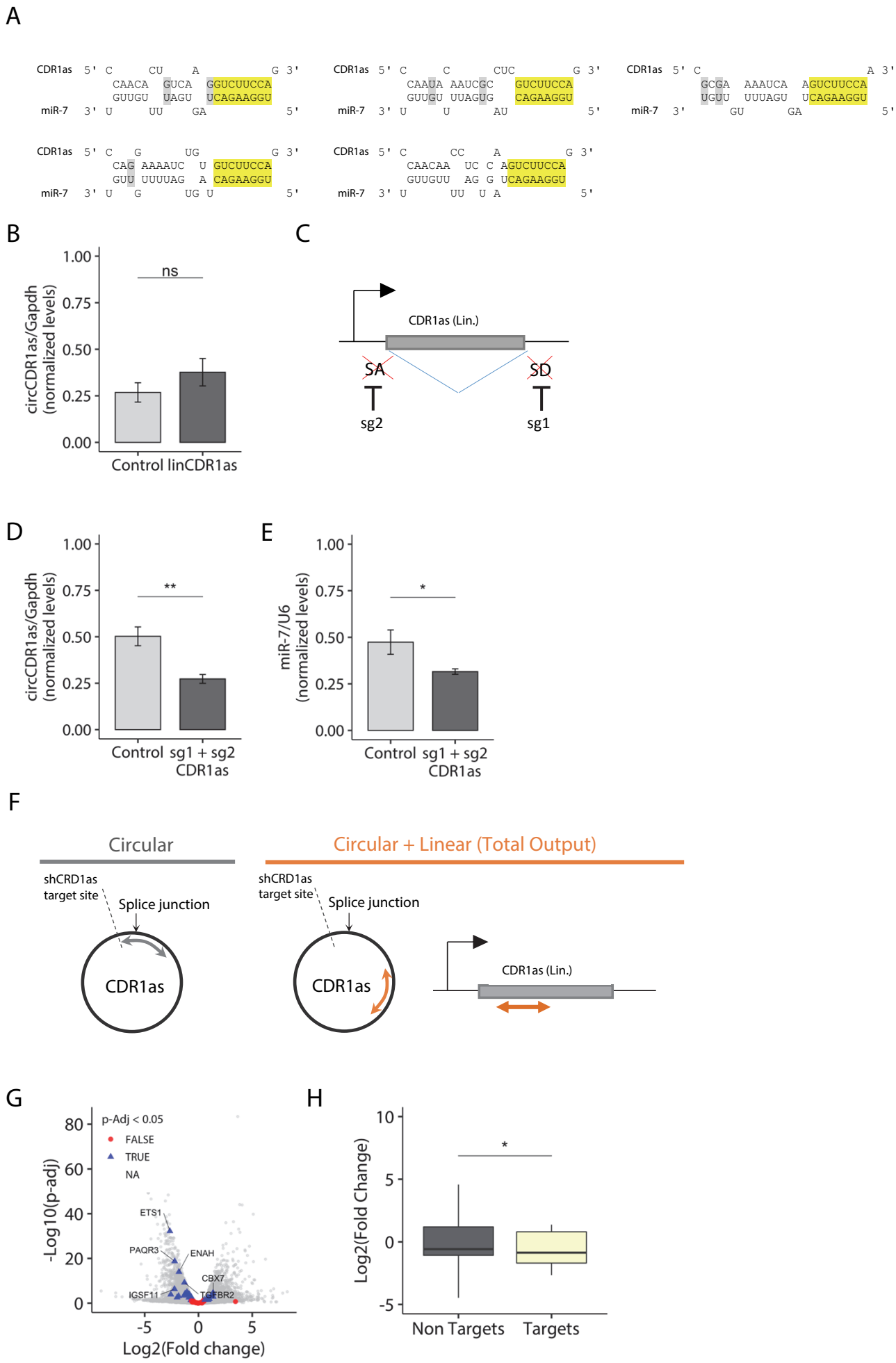
A
CDR1as 5' C CU A G 3'
CAACA GUCA GGUCUUCCA
GUUGU UAGU UCAGAAGGU
miR-7 3' U UU GA 5'
CDR1as 5' C C CUC G 3'
CAAUA AAUCGC GUCUUCCA
GUUGU UUAGUG CAGAAGGU
miR-7 3' U U AU 5'
CDR1as 5' C A 3'
GCGA AAAUCA AGUCUUCCA
UGUU UUUAGU UCAGAAGGU
miR-7 3' GU GA 5'
CDR1as 5' C G UG G 3'
CAG AAAAUC U GUCUUCCA
GUU UUUUAG A CAGAAGGU
miR-7 3' U G UG U 5'
CDR1as 5' C CC A G 3'
CAACAA UC C AGUCUUCCA
GUUGUU AG G UCAGAAGGU
miR-7 3' U UU U A 5'
B
circCDR1as/Gapdh (normalized levels)
1.00
0.75
0.50
0.25
0.00
ns
Control
linCDR1as
C
CDR1as (Lin.)
SA
SD
sg2
sg1
D
circCDR1as/Gapdh (normalized levels)
**
Control
sg1 + sg2 CDR1as
E
miR-7/U6 (normalized levels)
*
Control
sg1 + sg2 CDR1as
F
Circular
Circular + Linear (Total Output)
shCRD1as target site
Splice junction
CDR1as
shCRD1as target site
Splice junction
CDR1as
CDR1as (Lin.)
G
p-Adj < 0.05
FALSE
TRUE
NA
-Log10(p-adj)
80
60
40
20
0
ETS1
PAQR3
ENAH
CBX7
IGSF11
TGFBR2
-5
0
5
Log2(Fold change)
H
Log2(Fold Change)
10
5
0
-5
*
Non Targets
Targets

Figure S4

A

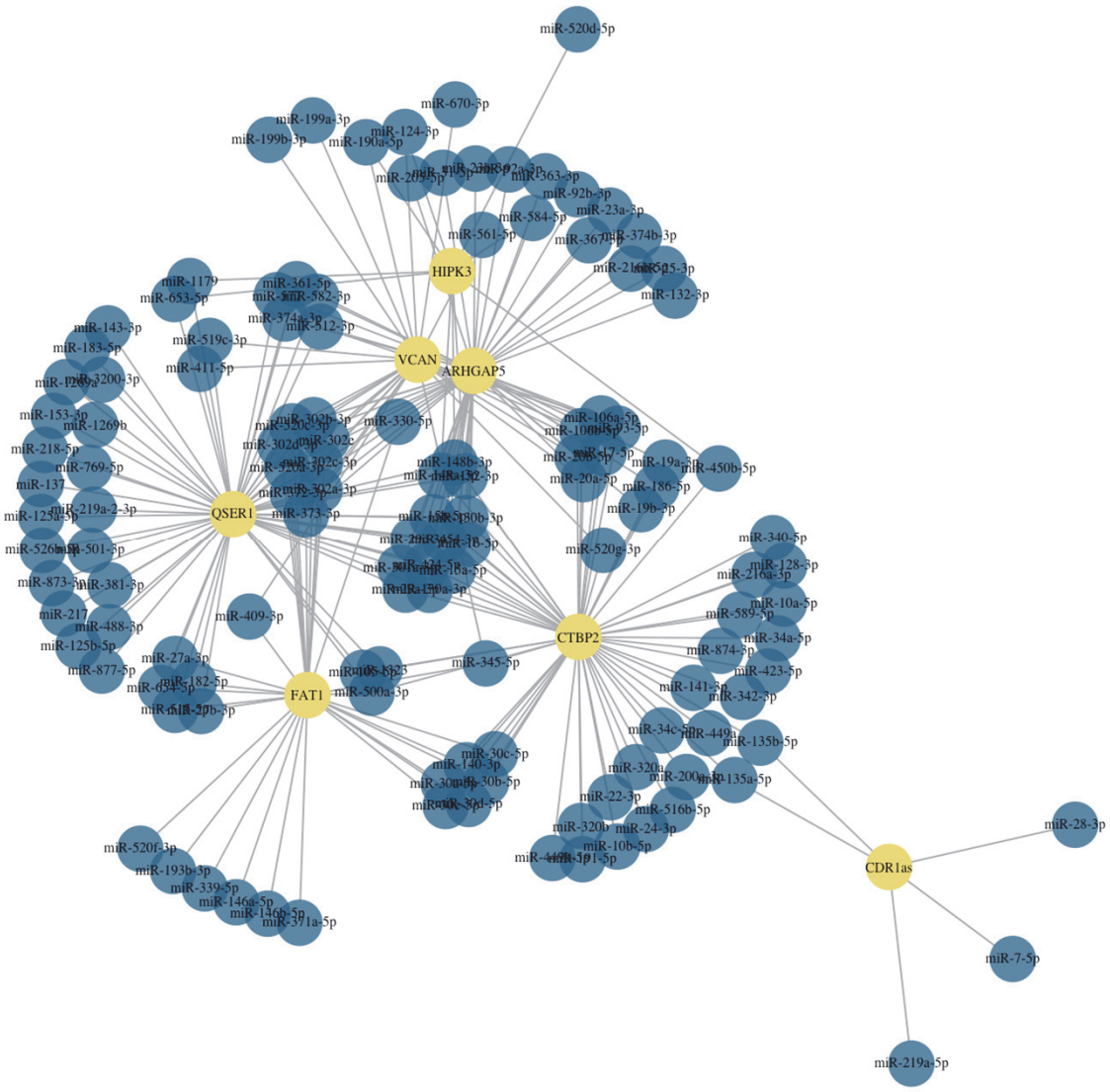
HIPK3
VCAN
ARHGAP5
QSER1
CTBP2
FAT1
CDR1as

B

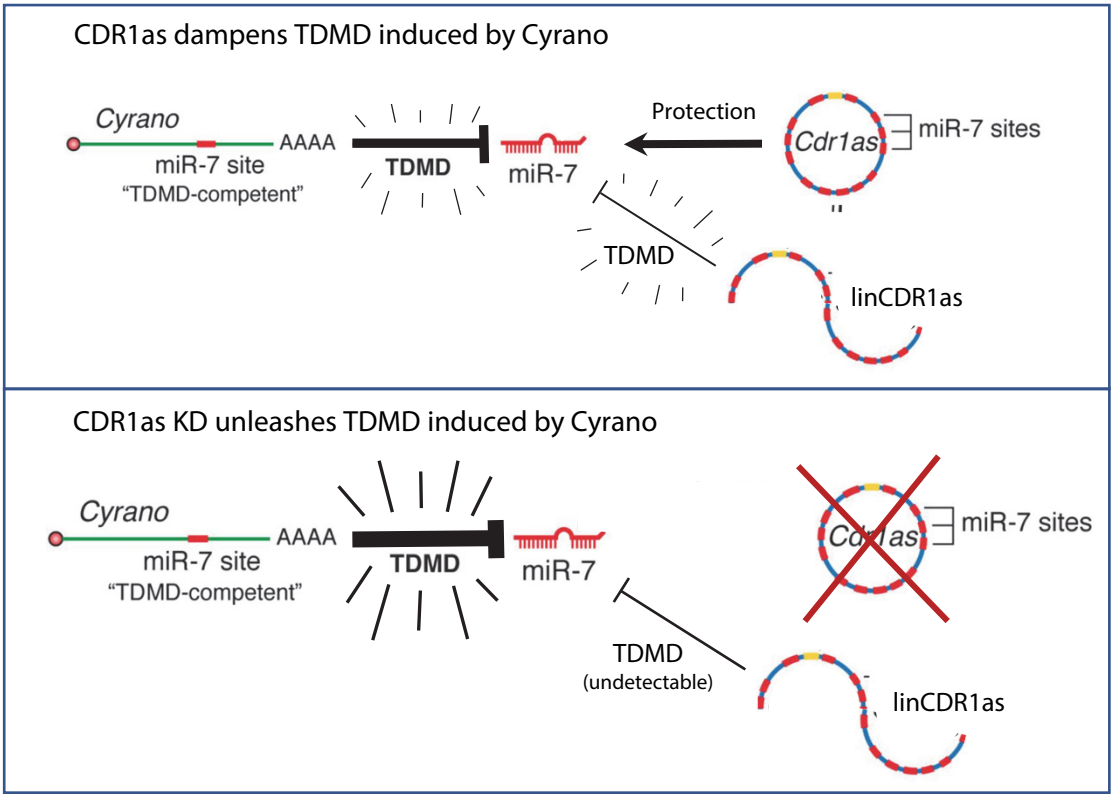
CDR1as dampens TDMD induced by Cyrano
Cyrano
AAAA
miR-7 site
"TDMD-competent"
TDMD
miR-7
Protection
Cdr1as
miR-7 sites
TDMD
linCDR1as
CDR1as KD unleashes TDMD induced by Cyrano
Cyrano
AAAA
miR-7 site
"TDMD-competent"
TDMD
miR-7
Cdr1as
miR-7 sites
TDMD
(undetectable)
linCDR1as

Supplementary Table 1

Oligo name	Use	Sequence 5'->3'
CiRS7_lin_For1	Linear CDR1as	gggtttccagtggtgccagt
CiRS7_lin_Rev1	Linear CDR1as	ctggatacggcagacaccag
ciRS7_lin_For_BamHI	Linear CDR1as lacking miR-671 site	atccGGATCCgggtttccagtggtgccagt
ciRS7_lin_Rev_SalI	Linear CDR1as lacking miR-671 site	atccGTCGACtgaaggaagacacatgtact
rno-miR-671-gblock_mouse-Cir7-match	shCDR1as	atagccgattagttctcgaggatccgggggcagatttgaccggcaggcatc agcagagggctgcttctacaacgctgactacctggcagcccgggcccggc tggctggtgaactggcaggccaggaagaggaggaagccctggagatgct ggaggtgatggatgttttcctccggtgttcagggctccacctctttcgagcc gtagagccagggctggtacagaagttctccctgagggactgcagcccccg gctcagtgaggaactgtaccaccgttgtcgcctcagcaacttggaggggct gctagctcgagcttttggagaatat
miR-7_Bulged_sites	Linear TDMD inducer miR-7 bulged	AGCTGTATAAGTAGGCTAGCCGTCACTGATATGCTCGAAC AACAAAATCTCCGTCTTCCATACAATTTAAAACCCGTCCCA CAACAAAATCACCGTCTTCCATATGCCCGTCCTCTCTCTTTA CAACAAAATCTACGTCTTCCACTTGCAAACCTCACTACAAT ACAACAAAATCGCTGTCTTCCAGTCGACAATCAACCTCTGG A
miR-7_Mut_sites	Linear TDMD inducer miR-7 mutated	AGCTGTATAAGTAGGCTAGCCGTCACTGATATGCTCGAAC AACAAAATCTCCGTACCACATACAATTTAAAACCCGTCCCA CAACAAAATCACCGTACCACATATGCCCGTCCTCTCTCTTT ACAACAAAATCTACGTACCACACTTGCAAACCTCACTACAA TACAACAAAATCGCTGTACCACAGTCGACAATCAACCTCTG GA
SZSCAN1_Ups_intron	Artificial circRNA	gagcgcagtcgagaggatccttttttttttttgacggagtttaacttcttgtctc ccaggtaggaagtgcagtggcgtaatctcggctcactacaacctccacctcc tgggttcaagcgtttctcctgcctcagctttccgagtagctgggattacaggc gcctgccaccatgccctgctgacttttgtatttttagtagagacggggtttcac catgttggccaggctggtcttgaactcctgaccgcaggcgattggcctgcct cggcctcccaaagtgctgagattacaggcgtgagccaccacccccggcctc aggagcgttctgatagtgcctcgatgtgctgcctcctataaagtgttagcag cacagatcacttttttgtaaaggtacgtactaatgactttttttttatacttcagga atagtaaagaaacacatcataaaacctcccaccggtcgccaccatggtga
SZSCAN1_Downs_intron	Artificial circRNA	taggggaagggaaatgattcaggacgagagtctttgtgctgctgagtgcct gtgatgaagaagcatgttagtgaaaagaattaggctcggcacggtagctca cacctgtaatcccagcactttgggaggctgaggcgggcagatcacttgagg tcaggagtttgagaccagcctggccaacatggtgaaaccttgtctctactaa aaatatgaaaattagccaggcatggtggcacattcctgtaatcccagctactc gggaggctgaggcaggagaatcacttgaacccaggaggtggaggttgca gtaagccgagatcgtaccactgtgctctagccttggtgacagagcgagact gtcttaaaaaaaaaaaaagtcgacaatcaacctctgga
pEGFP-miR_BclI_For	pri-miRs	CATCCTGATCATTTTTCGCAACGGGTTTGCC
GFP_Rev	pri-miRs	CTACTTGTACAGCTCGTCCATGC
TREp_XbaI_For	TRE promoter insert	CTACTtctagataggtttaccactccctatc
TREp_BamHI_Rev	TRE promoter insert	CATCCggatccCTAGGCGCGCCTTAATTAAG
sgCiRS7-1_For	sgRNA to mutate CDR1as splice sites	CACCGATGAAACAACTTTCAATACC
sgCiRS7-1_Rev	sgRNA to mutate CDR1as splice sites	AAACGGTATTGAAAGTTGTTTCATC
sgCiRS7-2_For	sgRNA to mutate CDR1as splice sites	CACCGATGATGTTTCCAATATCTAG
sgCiRS7-2_Rev	sgRNA to mutate CDR1as splice sites	AAACCTAGATATTGGAAACATCATC

Supplementary Table 2

Custom-made qPCR Mix	µL per Reaction
*10X Reaction Buffer **	2.5
MgCl2 25 mM	4
Triton x-100 10%	0.06
dNTP mix 10mM	0.5
Glycerol 60%	1.67
DMSO 100%	0.25
Betaine 5M	1.25
*Taq Polymerase (5 U/µL) ***	0.1
*SYBR Green (1/90)****	0.03
Primer Forward 10 µM	0.5
Primers Reverse 10 µM	0.5
H20	8.64
cDNA	5
Final volume	25

* 10X TAS reaction buffer from INBIO Highway

** Taq Polymerase from INBIO Highway

***SYBR Green (Sigma S9430).

***qPCR program:* 94°C-3′; (94°C-15′′; 60°C-15′′; 72°C-25′′) 40x, melting curve. All reactions were run in either an ABI Quantstudio 3 or an ABI StepOnePlus.

Supplementary Table 3

Oligo name	Use	Sequence 5'->3'
CiRS7_For5	Circular CDR1as divergent	cctacaactgcccagtgtctc
CiRS7_Rev2	Circular CDR1as divergent	ggtactggcaccactggaaa
CiRS7_For1	Circular + linear CDR1as (total output)	tgtgtcttccttcacctccag
CiRS7_lin_Rev1	Circular + linear CDR1as (total output)	ctggatacggcagacaccag
qWPRE_For	Linear CDR1as/artificial linRNA control exclusively	actgtgtttgctgacgcaac
qWPRE_Rev	Linear CDR1as/artificial linRNA control exclusively	caacaccacggaattgtcag
miR132 _Artificial_Circ_For	Circular artificial circRNA divergent	TACAAGTAAAGCGGCCGCGTCG
Artificial_Circ_Rev	Circular artificial circRNA divergent	CTCGCCCTTGCTCACCATGGTG
mCherry_seq_For	Circular + linear artificial circRNA (Total output)	gtggaacagtacgaacgcgcc
Linker-2_BsrGI_Rev	Circular + linear artificial circRNA (Total output)	CTACTTGTACATATGATTAGTGGTTTAAA
ZSCAN1_down_Seq_Rev	Linear artificial leak exclusively (combined with Artificial_circ_For)	TGAGCTACCGTGCCGAGCCTAA
Klf4f	miR-7 Target	aaaagaacagccaccacac
Klf4r	miR-7 Target	tcccagtcacagtggtaagg
Egr3f	miR-7 Target	cgcgctcaacctcttctc
Egr3r	miR-7 Target	attgggcttctcgttggtc
Irs2f	miR-7 Target	gagtgtgtgggggtccag
Irs2r	miR-7 Target	aatgtagaattgctcccgttg
Nr4a3f	miR-7 Target	tgcctgtcagcactgagtatg
Nr4a3r	miR-7 Target	agagcctgtcccttcctgt